CHAPTER 7

Measurement and analysis of polarisation effects in optical fibres with a polarimetric OTDR

The principle of time domain reflectometry (TDR) may be dated back to the 1930's [187] where, in electrical measurement, a transmitter sends a pulse along a coaxial cable and a receiver and oscilloscope monitor the echoes returning back to the input. Optical TDR was first demonstrated by Barnoski and Jensen in 1976 in multi mode fibres [17] and over the years, it has proved to be an invaluable diagnostic tool for use in both multi mode and single mode optical fibre systems to measure fibre loss, splice losses, locate faults, etc. Nowadays, OTDRs are available from many manufacturers with spatial resolutions as small as one metre. The original principle of POTDR was first proposed by Rogers in 1980 [16] showing that POTDR can measure the birefringence characteristic along fibres with access to only one end. POTDRs, unlike OTDRs, are currently not commercially available and the reasons are various: one is the higher demand on the spatial resolution performance compared to conventional OTDR (as will be discussed) and also the lack of mass commercial interest. However, as stated above, powerful OTDRs are available nowadays and with the growth of interest in PMD, there is now a corresponding interest in an instrument which can measure birefringence (PMD) along a fibre with access to only one end[1]. Moreover, up to now, the analysis of POTDR traces have ignored twist, and given that twist has a large influence on the DGD of the fibre (Chapter 5 and 6), analysis of the influence of twist on the backscattered SOP has been carried out.

The experimental techniques used have developed through the following stages. At first, the performance of a basic OTDR was enhanced through the use of erbium amplifiers. This *enhanced* OTDR was then converted into a *single-channel* polarimetric OTDR. Finally, some measurements are reported using a novel *four-channel* polarimetric OTDR.

The structure of this chapter is as follows. Section 7.1 introduces the conventional OTDR and progresses to the experimentally used optically amplified enhanced OTDR which has been modified to a polarimetric OTDR to measure the backscattered SOP evolution. The OTDR-POTDR performance parameters will be defined and are measured for the used POTDRs. Section 7.2 derives the matrix description of the backscattered SOP evolution in twisted fibres

which allows calculation of the local birefringence in the presence of twist. Two analytical equations which define the backscattered SOP evolution will be given which describe the periodicity and the SOP evolution and the shape of the SOP evolution on the Poincaré sphere. The equation defining the periodicity of the SOP evolution is especially useful if using just a fixed polariser to analyse the fibre birefringence. Furthermore, a vector equation will be derived describing the backscattered SOP evolution which can be easily implemented for computing and fast analysis of the POTDR waveforms. Section 7.3 shows the measurement results with computational analysis using the single-channel POTDR on fibres with different twist rates. The birefringence will be calculated from the POTDR data and from that the DGD is estimated. The DOP of the backscattered light which is lower than expected (~80%) will also be considered. Section 7.4 introduces the four-channel POTDR with some more measurement results which confirmed the validity of the theory. The effect of random mode coupling on the POTDR waveform will also be shown. Section 7.5 gives a list of the DGD values estimated with POTDR data with the offset from the measured DGD values in Chapter 6. The error in the measured backscattered SOP are categorised into periodicity error and error in the shape of the SOP evolution on the Poincaré sphere. Finally, the desired two-point resolution for POTDR as a function of the fibre birefringence will be discussed.

7.1 OTDR and POTDR performance parameters

7.1.1 Conventional direct detection OTDR

A general outline of a direct detection OTDR is shown in a schematic diagram in Figure 7.1. A pulse from an laser source driven from an electrical pulse generator is launched over a directional coupler into an optical fibre where the pulse undergoes Rayleigh scattering along the fibre (Section 2.5). The backscattered power is then separated from the launched signal via a directional coupler to an optical detector (usually APD) which converts the optical signal to an electrical signal. The electrical signal is then amplified, digitised by an A/D converter and averaged in the signal processing unit to improve the signal-to-noise ratio. Finally, the backscattered signal is displayed as a function of time (distance) in logarithmic form. The repetition rate of the pulse must be chosen such that the signals returning from the fibre do not overlap. This is typically from 1 to 20 kHz depending on fibre length.

[1] Commercial interest after publishing the work described in this chapter has been shown by various manufacturers of optical instruments.

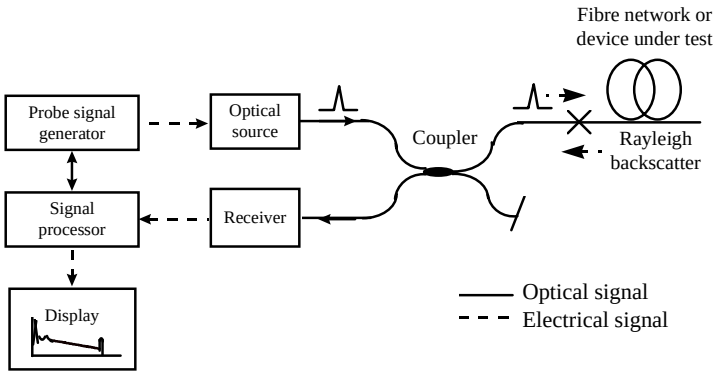

Figure 7.1 Schematic of direct detection OTDR

7.1.1.1 Enhancements of OTDR performance

Dynamic range, spatial resolution and noise reduction are the main features characterising the performance of an OTDR, and will be defined in Section 7.1.4 for basic OTDR and the polarisation OTDR. The majority of commercially available OTDRs use direct detection as described above because of its simplicity, straightforward optical and electrical design, simple signal processing, relatively low cost and low coherent effects [188]. However, there is a trade-off between dynamic range and resolution in using a conventional direct detection OTDR which is mainly imposed by the receiver noise [188]. Two kind of techniques have been proposed and pursued over recent years to enhance OTDR performance, which can be classified as (i) decreasing the minimum detectable power and (ii) increasing the input optical power.

(i) The receiver sensitivity can be enhanced by the use of (a) correlation, (b) coherent detection, (c) photon counting OTDR, etc. [188]-[190].

(a) Correlation OTDR uses a pseudorandom bit sequence as the modulating signal and a cross correlator performs time correlation between the electrical reference signal, which can be delayed, and the optical backscattered signal.

(b) Coherent OTDR based on heterodyne detection uses a narrowband source (e.g. external modulated DFB laser with frequency shift using an acousto-optic switch) which is mixed with the backscattered signal in the photodetector. In using coherent detection, the dynamic range is increased (quantum-limited sensitivity), but suffers effects like coherent speckle (interference from the scattering points along the fibre), phase noise from the laser itself and polarisation fading which gives rise to undesired fluctuations in the backscattered signal. This polarisation fading and polarisation noise in conventional direct detection OTDR is the information used in polarisation OTDR to measure the evolution of polarisation in the fibre. In coherent OTDR, polarisation

fading and speckle fluctuation are reduced by employing polarisation and frequency scrambling which adds further to the complexity of coherent OTDR.

(c) Photon counting OTDR showing centimetre resolution with high sensitivity, by using pico second pulses in combination with a single-photon avalanche detector [189], would be the optimum choice for a POTDR when measuring short lengths of fibre[2]. However, the relatively long measurement time and very high purchase price are drawbacks.

(ii) Enhancement of optical power can be achieved by using high power sources like a Q-switched Er^{3+} glass laser at 1.55μm. Another very attractive method for increasing OTDR performance is to employ erbium-doped fibre amplification of both the transmitted pulse and the backscattered signal [191]-[193]. Optical amplification using a boost amplifier has been used in the single-channel POTDR to enhance the output power of a conventional direct detection OTDR. However, there is a non-linear power limitation in the maximum probe pulse power due to non-linear scattering caused by stimulated Raman and Brillouin scattering (Section 2.5). The critical peak power limit at λ = 1.55 μm using highly coherent sources, has been given in [188] for Raman scattering as larger than +34 dBm and for Brillouin scattering for pulsewidths < 1 μs as larger than +28 dBm[3].

7.1.2 Enhanced OTDR using erbium doped fibre amplifiers

Erbium doped fibre amplifiers give not only a significant advance in lightwave communication systems but also in optical devices, as mentioned above for OTDR, to increase the output power or minimum detectable power of the device. For the single-channel polarisation OTDR such an enhanced high resolution large dynamic range OTDR was directly available to us for the experiments [192]. The enhanced OTDR consists of a commercial OTDR with boost amplifiers and control box with an optical switch to prevent amplified spontaneous emission (ASE) from the erbium amplifiers entering the fibre when there is no pulse.

---

[2] A demonstration of a commercial photon counting OTDR with centimetre resolution working at 1.55μm from Opto-Electronics Inc., Canada modified to a POTDR (with fibre polariser) has been demonstrated at Essex University in May 96 (Purchase price ~ £90.000).

[3] OTDR action: large repetition rates (~ 1 to ~20 kHz), average power is very low.

7.1.2.1 Experimental OTDR set-up

A block diagram of the enhanced OTDR set-up is shown in Figure 7.2. It consists of a commercially available high resolution OTDR modified with a DFB laser and erbium amplifiers to extend the dynamic range. The main frame (Anritsu OTDR MW 920A at 1.55 μm) drives the laser and performs the optical to electrical conversion with digital averaging of the backscattered signal. The available pulsewidths are 6, 25 and 160 ns and the repetition rate of 2.5 kHz and 1.25 kHz is set by the distance range (DR) of 15 km and 40 km respectively. The external DFB laser has a centre wavelength at 1.55 μm with peak output power of 0 dBm. The erbium-doped amplifiers, developed at BT Laboratories, are used as power amplifiers to amplify the peak output power from the DFB laser from 0 dBm to +11 dBm with commensurate increase in the two way dynamic range. Optical isolators are used to protect the DFB laser and to prevent lasing of the amplifiers from external reflections.

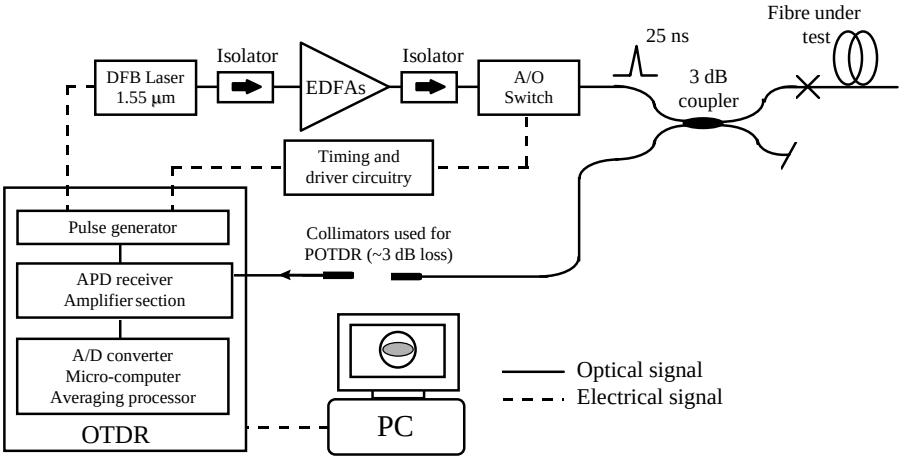

Figure 7.2 Block diagram of modified OTDR with DFB laser and erbium doped amplifiers.

The acousto-optical switch (AOS) works as a filter in the time domain, being synchronised to open as the amplified pulse reaches the appropriate part of the transmitter, thus allowing only the amplified pulse to pass and preventing receiver saturation from amplified spontaneous emission (ASE) noise and pump laser power. The extinction ratio of the switch is larger then 35 dB. The optical pulse is then passed through a coupler (polarisation insensitive) separating the transmit and receiver path. The backscattered light after passing the collimators (which will be used for POTDR), is then detected by an avalanche photo diode within the main frame of the OTDR. The bandwidth (*BW*) of the optical detector and amplifier section after the optical detector is about 80 MHz. The backscattered signal is (after A/D conversion) averaged in 501 buckets which are the sample points along the measured fibre length. The data can be accessed using the OTDR GPIB interface and a computer to analyse the backscattered data.

Figure 7.3(b) shows the measured OTDR trace on a ~1.7 km single mode fibre using the enhanced OTDR as shown in Figure 7.2, with pulsewidth of 25 ns and no averaging. It can be seen that the single way dynamic range is about 3.5 dB without any averaging. The one way dynamic range is half the two way dynamic range if measured on the OTDR screen, because the OTDR displays the one way fibre attenuation and a division by 2 is performed in the vertical scale.

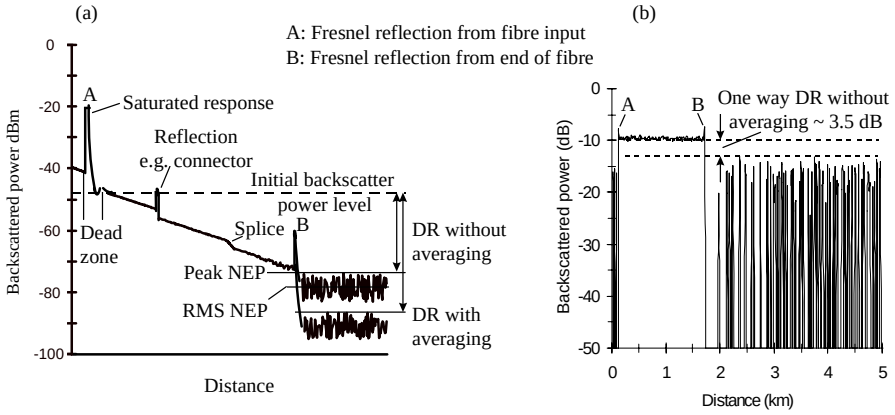

Figure 7.3 In (a) sketch of OTDR waveform with different losses and the effect of averaging on the DR. In (b) trace of enhanced OTDR (with collimators in return path) measured on ~1.7 km single mode fibre with 25 ns pulsewidth and without averaging.

The external DFB laser in the OTDR set-up in Figure 7.2 has been used to obtain a well polarised output SOP (DOP > 94% see Section 7.1.5) which is essential for POTDR. This was necessary because using the internal Fabry-Perot laser (inside the OTDR) with its broad spectrum[4] required a fibre polariser to be inserted in the output path of the OTDR due to depolarisation by the 'poor' isolators[5] which had high PMD values. Using the fibre polariser to polarise the depolarised pulse incurs an additional loss of about 4 dB (including insertion loss). The majority of POTDR measurements have been performed by using the DFB laser. In Appendix B, there is also a measurement shown by using a Fabry-Perot laser with fibre polariser at the output.

The DFB lasers large coherence length is also of benefit if measuring long fibre lengths of fibre because of its lower sensitivity to pulse broadening due to fibre dispersion compared

[4] The envelope of the Fabry-Perot laser spectrum has been measured to have a 3 dB width of ~ 12 nm whereas for the DFB laser the 3 dB linewidth can be taken as less than 100 MHz.
[5] These old isolators showed PMD values around 5 ps but were the only ones available to us at that time.

with the Fabry-Perot laser. Furthermore, for POTDR applications, the pulse remains polarised over greater lengths of the measured fibre.

7.1.3 Experimental polarimetric OTDR set-up

Polarisation OTDR has been demonstrated in the laboratory with various configurations being used to extract the polarisation information from the backscattered trace. A simple way of extracting the polarisation information is by placing a polariser in the receiver path of the OTDR, as for example, in [194]-[196]. The polarisation information in the backscattered intensity can also be observed by simply placing a fibre polariser between the OTDR output and the fibre under test where the polariser for the launched pulse acting as a polariser and for the backscattered light as an analyser. However, by using just a polariser only one Stokes component of the polarised light is obtained (Chapter 4), and in order to extract the full information contained in the backscattered SOP, a general compensator analyser combination has to be used as discussed in Chapter 4 for polarimetry. In [197], a polarimetric OTDR has been demonstrated to obtain the full Stokes vector by using an electro-optic modulator and rotating polaroid filter (sheet polariser) combination at $\lambda \sim 0.5$ μm.

Next, the modification of the enhanced OTDR in Figure 7.2 will be shown by simple polarimetric means as discussed in Chapter 4. It should be noted that although optical amplification is used to enhance the dynamic range in the relatively ‘old’ OTDR (made in 1990), the following method described could be directly used to extract the backscattered SOP information in modern high resolution conventional OTDRs if they possess a single way dynamic range of at least 10 dB.

7.1.3.1 The modification for analysing the backscattered SOP

The enhanced OTDR has been transformed to a polarimetric OTDR by using a computer controlled $\lambda/4$ waveplate-linear polariser combination, placed between the two collimators in the receiver path of the OTDR, Figure 7.4. The SOP from the backscattered intensity containing the polarisation information, could be calculated by rotating the $\lambda/4$ plate to at least four independent positions, for example, –30, 0°, 30° and 60°, as discussed in Section 4.2. In the following experiments, the $\lambda/4$ plate has been rotated to 19 analyser positions from 0° to 180°, and the backscattered SOP calculated from the measured intensities using a least square identification [165]. This improved the calculated SOP considerably, compared to just using four analyser positions, due to noise reduction in the individual Stokes components. However, the measurement time increases and in fibres, where the SOP is not stable, for example, aerial cables (ground wire of electricity pylons), it may be preferable to use no more

than four analyser positions. Rotation of the polariser has been avoided because of the beam deflection which would lead to an error in the analysed SOP (see Subsection 4.3.5). The measurement time for one set of measurement results to obtain the backscattered SOP is about 30 minutes, which includes rotating of the λ/4 plate to 19 analyser positions, averaging and data transfer to the computer.

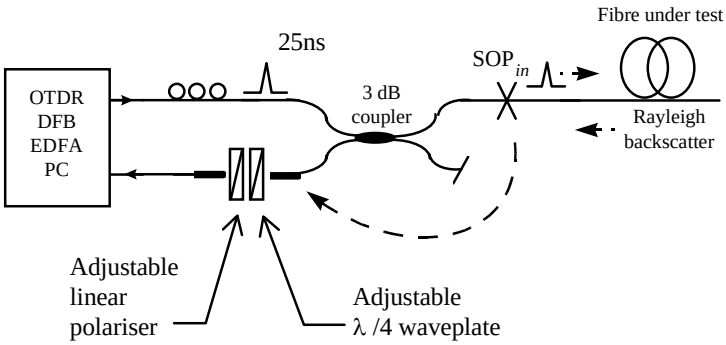

Figure 7.4 Single-channel polarimetric OTDR set-up.

Using a DFB laser means that the input pulse is well polarised and the polarisation controller at the output path before the 3 dB coupler could be used to control the input SOP. The data stored in the OTDR for every $\lambda/4$ plate position after averaging is accessed by the computer through the OTDR GPIB interface, which analyses the linear fluctuation and calculates and displays the SOP evolution along the fibre. Figure 7.5 shows the backscattered trace measured on a short length of S-SMF (at zero twist) for a pulsewidth of 25 ns, using the OTDR as shown in Figure 7.4 with and without polariser. The peak-to-peak amplitude of the fluctuation with the polariser is up to 10 dB whereas without it, the difference between minimum-maximum value is about 1 dB. The small fluctuation observed without the polariser is most probably due to a combined effect of intensity fluctuation due to variation of the scattering points along the fibre (coherent effect), polarisation sensitivity of the receiver and receiver noise. This small fluctuation, if not due to polarisation 'noise' and slowly changing over measurement time, will lead to an error in the POTDR results. The fluctuation measured

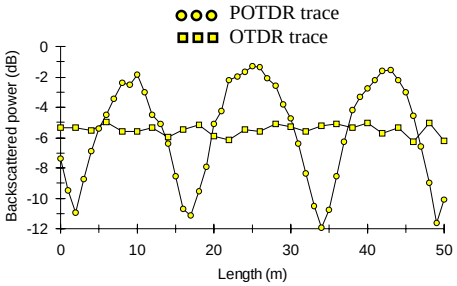

Figure 7.5 Typical OTDR and POTDR waveform from a short length of fibre. Measure on a S-SMF at zero twist with 25 ns pulsewidth and 1.5 minutes averaging.

with polariser (Figure 7.5) has been obtained by varying the input SOP and quarter waveplate-polariser axis orientation to obtain maximum fluctuation.

7.1.3.2 Review of work on polarisation OTDR in the literature

Reported POTDR application and measurement results in the past may be grouped into (i) theoretical work, (ii) sensor applications by analysing the backscatter in single mode fibres and neglecting twist, (iii) measuring of linear birefringence, (iv) determination of mode coupling in HiBi fibres and (v) estimation of PMD.

(i) A mainly theoretical treatment for analysing the birefringence from the backscattered light, but assuming only linear birefringence, can also be found in [16], [198]-[200], where the first three references also consider practical measurement limitations and factors affecting the sensitivity and accuracy of POTDR.

(ii) The POTDR has been extensively treated for sensing applications such as electric and magnetic fields and temperature monitoring [201]-[204], where its effectiveness in the presence of magnetic fields has been demonstrated in [205].

(iii) The fibre birefringence along an optical fibre has been estimated from the backscattered POTDR signal. In analysing the power spectrum from the POTDR fluctuation [195], one sharp peak was observed and related to the polarisation beat length, but with no mention of twist in the fibre. Reference [206] showed that by bending a fibre around a small diameter drum without twisting, the linear birefringence due to bending (Subsection 3.3.7) can be estimated from the POTDR fluctuation. In [197], a polarimetric OTDR at $\lambda \sim 0.5$ μm has been used to obtain the full Stokes vector and to estimate the linear birefringence in the fibre. It was mentioned that circular birefringence (which cannot be totally avoided) could influence the measurement results but the effect of twist on POTDR signal was not considered any further. In [207], an interesting method of downshifting the measured POTDR fluctuation by optical beating of the backscattered signal from two lasers was demonstrated, reducing the minimum measurable fluctuation due to the receiver bandwidth.

(iv) Mode coupling along high birefringence fibres has been analysed [208] and measured using POTDR [209], [210]. The input SOP has been aligned with one of the principal axes of the fibre and the backscattered light has been analysed through a rotatable polariser at 0° and 90° to the principle axes of the HiBi fibre.

(v) Detection of sections with large PMD by using POTDR with a single polariser in the receiver path. The methods include counting the periodicity in the POTDR fluctuation [196], observing the power spectrum from the fluctuation [211], [212], and trying to

identify from the magnitude of the POTDR fluctuation, fibre sections where the launched pulse is strongly depolarised, which would correspond to a high PMD [213]. In the references [196], [211]-[213], the fibre is assumed to possess only linear birefringence.

In the above literature, it has often been assumed that a fibre may be described as a system of linear retarder-rotator combinations, and for the light travelling in reverse direction, the rotator is reversed and is cancelled. However, this assumption is not valid for twisted fibres because although the circular birefringence induced by twist cancels for the combined forward-backward transmission (see Section 6.2), there is also a geometrical rotation of the local linear birefringence. It will be shown from Section 7.2 onwards, theoretically and by measurement, that even a small amount of twist can have a large influence on the POTDR fluctuation, and if neglected, leads to a large error in the estimated birefringence and DGD [15] [170] [214] [215].

7.1.4 Performance parameters of the POTDR

This section treats at first the backscattered optical power from a single mode fibre. From that, the main performance parameters for OTDR and POTDR will be discussed and given for the single-channel polarimetric OTDR. The parameters considered are the dynamic range, the spatial resolution and a more POTDR specific parameter, the DOP of the launched pulse and its repeatability with time. These performance parameters will determine the error in the measured backscattered SOP and the POTDR waveform periodicity and will be reconsidered at the beginning of Section 7.3 which treats the measurement results.

7.1.4.1 Backscattered mean power

The Rayleigh backscattered power P_R in a step index fibre from a rectangular optical pulse with a width W and peak power P_0, observed at the input end of the fibre at the time t is [216]

$$P_R(l) = \frac{1}{2} S \alpha_s W v_g P_0 10^{-\frac{\alpha}{10} v_g t} \tag{7.1}$$

where S is the backscattering capture coefficient, α_S the loss coefficient due to Rayleigh scattering which is about 0.18 dB/km for pure silica (Equation 2.24), but depends also on the doping level, W is the pulsewidth, α is the fibre loss coefficient which is about 0.2 to 0.25 dB/km at λ = 1.55 μm in single mode fibres and v_g the group velocity. The group velocity in a fibre is defined by Equation 3.10 as $v_g = c/n_g$ and for simplicity, we may assume n_g is

constant, so that c/n represents approximately the light velocity in the fibre and the time t corresponds to the position $l \approx ct/(2n)$ in the fibre, with $2\alpha l$ the round trip loss.

Figure 7.6(a) shows the initial Rayleigh backscattered power at $l = 0$ as a function of the pulsewidth W by using Equation (7.1). The ratio of the backscattered power to the input power $P_R(0)/P_0$ has been plotted by using α = 0.2 dB/km, α_S = 0.04 /km and $S = 1\times10^{-3}$ which are some typical values for S-SMF at 1.55 μm. Figure 7.6(b) shows the measured backscattered power from a S-SMF as a function of the input peak power for a pulsewidth, W, of 10 ns. The backscattered power increases linearly with increasing input power as would be expected from Equation (7.1) for Rayleigh scattering because the launched power is below the power threshold for stimulated Brillouin and Raman scattering (Subsection 7.1.1.1). The backscattered power has been measured using a 6 GHz optical receiver with a 20 GHz sampling oscilloscope.

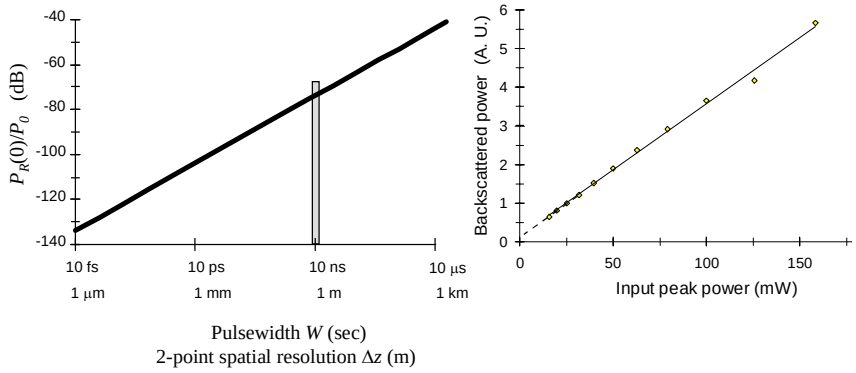

Figure 7.6 In (a) backscattered power calculated versus the pulsewidth W with the two-point resolution of the pulsewidth $\Delta z \approx Wv_g/2$. In (b) backscattered power measured versus input peak power for a 10 ns pulse lunched in a 60 metre fibre.

7.1.4.2 Dynamic range in dB

The two way optical dynamic range (DR) for OTDR (POTDR) can be defined as the difference of the initial (highest) Rayleigh backscattered power $P_0(0)$ to the minimum detectable returned power. This equates to double the one way loss tolerated along a fibre before the trace is indistinguishable from the noise, which is mainly internal from the instrument but may also be scatter noise and, if using erbium amplifiers, ASE noise. The minimum detectable power could be specified as the RMS based NEP of the receiver (SNR = 1) but more commonly in OTDR specification, the peak noise amplitude is taken which may

be taken as about 3 times larger than the RMS value (3σ for Gaussian noise with zero mean). The two way DR can be expressed as

$$DR\,(dB) = 10\log\left(\frac{P_R(0)}{NEP_{Peak}}\right) = P_R(0)\,(dBm) - NEP_{Peak}\,(dBm) \qquad (7.2)$$

The one way DR including the factor 2 for round trip loss is half the DR specified in Equation (7.2) and can be directly obtained from the OTDR display as indicated in Figure 7.3 (a) and (b), which automatically includes all the noise contributions and also the loss due to the coupler. For POTDR applications with an analyser in the receiver path and short fibre lengths (< 1 km), so that the fibre loss can be neglected, the two way dynamic range is important and will determine the noise error in the measured SOP (Section 4.4).

Averaging of the backscattered signal after repetitively measuring over many pulses improves the SNR. The arithmetic average of the samples can be generated by using an analogue method (boxcar averaging), or by digital averaging after the A/D conversion is performed (Figure 7.2). Assuming Gaussian distributed noise, the reduction in NEP is proportional to the inverse square root of the number, *N*, of measurements [188]

$$NEP_{Av} = NEP/\sqrt{N} \qquad (7.3)$$

For a 20 dB noise suppression, a time averaging of 10^4 values would be needed (Equation (7.3)), but in practice the improvement in the SNR will saturate through effects like the quantization noise from the A/D converter if using digital averaging, and also drift in the receiver.

Figure 7.7(a) shows the two measured pulsewidths from the used OTDR shown in Figure 7.2, after amplification, measured with a fast receiver and oscilloscope. The full width half maximum (FWHM) of the two pulses are about 6 and 25 ns with peak powers of about 11 dBm. Figure 7.7(b) shows the measured two way DR of the used POTDR (Figure 7.4 without polariser and λ/4 plate) as a function of averaging time. The DR has been obtained from the OTDR display as shown in Figure 7.3(b), by measuring the difference in the initial Rayleigh backscatter power to the highest observed noise peak power. By measuring the DR in this way, the losses due to the 3 dB coupler, and due to the collimators are taken into account in the DR. For POTDR an additional loss, due to the intrinsic loss of the λ/4 plate and polariser, of < 0.5 dB has to be subtracted from the DR shown in Figure 7.7(b). The averaging time

used in the backscattered SOP measurements (Section 7.3) is 1.5 minutes in order to keep measurement time reasonable and still have a reasonable noise reduction. For 1.5 minutes averaging time, the DR for the 25 ns pulse is about 21 dB and about 9 dB for the 6 ns pulse. In Section 4.4, it has been shown that in order to keep the error reasonable in the measured SOP, the SNR should be above 10 dB (Figure 4.9, $\varepsilon < 20°$) which is why for the single-channel POTDR the 6 ns pulse was not used, although it would give a higher resolution.

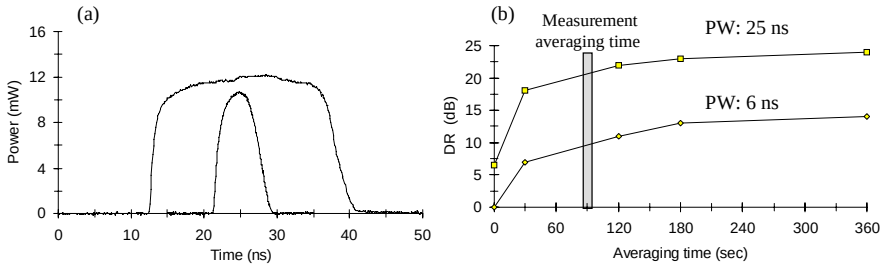

Figure 7.7 DR increase with averaging In (b) for 25 ns pulse two way DR ~ 20 dB for 90 second averaging.

7.1.4.3 Principle error sources

The absolute distance resolution which may be calculated from $l \approx ct/(2n)$ depends on the fibre refractive index which may change slightly from fibre to fibre, and further depends on the accuracy and stability of the instrument time base (sampling resolution). For short distances, the error in the time base will be dominant, whereas for long distances, it is the error in the refractive index. However, for the reported POTDR measurements, we are only interested in short distances and the relative difference between measurement points is of more importance and will be treated in Subsection 7.1.4.4.

The accuracy and linearity of the vertical scale depends not only on internal parameters of the OTDR, such as the linearity of the amplifiers and the quantization noise induced by the A/D converter, but also on the SNR and noise in the scattered intensity, such as polarisation and coherent scatter noise. For POTDR, the dominant error source in the vertical scale is the limited SNR as shown in Figure 7.7(b), and also some small fluctuation as observed in the measured OTDR intensity in Figure 7.5 which is not due to just polarisation noise.

7.1.4.4 Two-point resolution in metres

The two-point resolution (spatial resolution) is a measure of the closest spacing between two fibre discontinuities which the OTDR (POTDR) can separate. Assuming sufficient SNR to

separate the signal from the noise, the two-point resolution, Δz, is dependent upon the pulsewidth *W*, and impulse receiver response time t_r, and is calculated from [188]

$$\Delta z \approx \frac{v_g}{2}\sqrt{W^2 + t_r^2} \tag{7.4}$$

The receiver response time may be taken as equal to the inverse of the detector bandwidth *BW*, $t_r = 1/BW$. Ideally, Δ*z* should be small (short pulsewidth and large receiver bandwidth) but as can now be seen, in comparing Equation (7.4) with Equation (7.1), there is a trade-off between the two-point resolution and the SNR. For the used OTDR, the 3 dB cut-off frequency is about 80 MHz which for the 25 and 6 ns pulse gives an estimated two-point resolution from Equation (7.4) of about 2.8 and 1.4 metres respectively. For the calculation of the two-point resolution in the fibre, a rectangular pulse is assumed and fibre dispersion contribution to the pulsewidth has been neglected which is valid for short fibre lengths.

A direct measurement of Δ*z* may be obtained from the OTDR display by measuring the FWHM value of the pulse response from one reflection point in the fibre which in the logarithmic scale is −3 dB from the maximum measured backreflected power. Figure 7.8 (a) and (b) show the measured reflection from a fibre back to back connection measured with the enhanced OTDR for the 25 and 6 ns pulsewidth respectively. Saturation has been avoided and the − 3 dB points are about 2.5 and 1.2 metre for the 25 and 6 ns pulsewidth respectively, which is only slightly less then expected from the theoretically estimated values above.

Figure 7.9 shows the OTDR response for the 25 and 6 ns pulsewidth for reflection from two reflection points, which was constructed using two back to back connectors separated by 3, 2.6 and 2 metre fibres. It can be seen in Figure 7.9(a), that the 25 ns pulse can just resolve the two reflection points which are 2.6 metres apart, showing a dip of about 0.5 dB in the centre part, whereas the 6 ns pulse, as expected from the estimated and measured value above, can still resolve the two reflection points which are 2 metres apart showing a dip of about 6 dB.

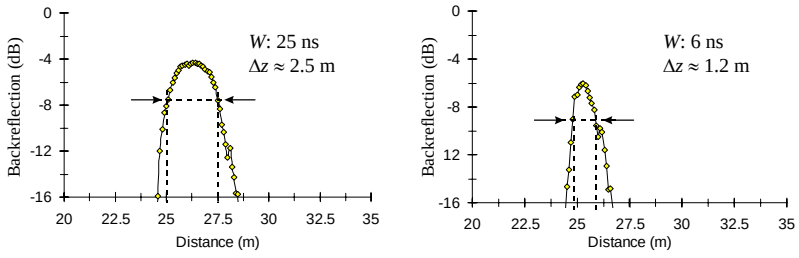

Figure 7.8 Measurement of the OTDR (POTDR) two-point resolution from one reflection point as the FWHM value. In (a) for 25 ns pulsewidth and in (b) for the 6 ns pulsewidth.

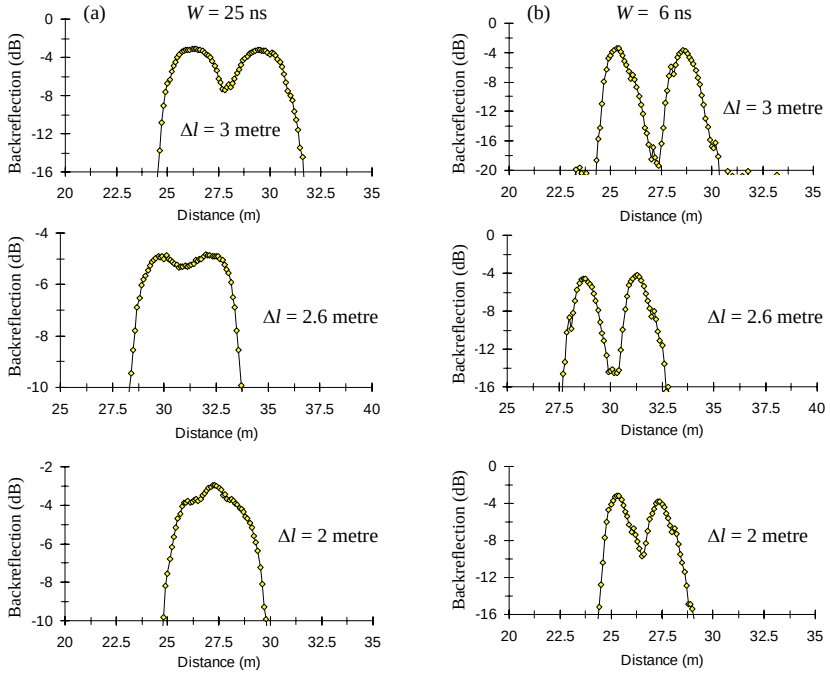

Figure 7.9 Measurement of the OTDR (POTDR) minimum resolution of two reflection points. In (a) for 25 ns pulsewidth and in (b) for the 6 ns pulsewidth.

7.1.4.5 Degree of polarisation and repeatability with time of the output pulse

The DOP of the output pulse from the enhanced OTDR has been measured which (ideally for POTDR application) we would like to have fully polarised in order to minimise error in the measured SOP in the presence of noise (see Section 4.4). This is in contrast to OTDR applications where a low DOP is desired in order to reduce polarisation noise in the OTDR waveform. Figure 7.10 shows the measurement set-up used for measuring the DOP of the output pulse from the enhanced OTDR. The DOP of the output pulse has been measured using a broadband receiver and sampling oscilloscope by searching for the minimum and maximum power transmission through the linear polariser with a polarisation controller. Figure 7.11 (a) and (b) shows the obtained maximum and minimum power transmission which shows an extinction ratio of about 15 dB between the peak values. The DOP is given by (Equation 2.12) DOP = $(P_{max} - P_{min})/(P_{max} + P_{min})$ so that from Figure 7.11 (a) and (b), the DOP of the output pulse is > 94%. Figure 7.11 (b) also shows that the SOP of the pulse time

changes at t_{on} and t_{off}, but this SOP change is relatively small (< 10° on the Poincaré sphere) because of the sensitivity to SOP change at minimum power transmission.

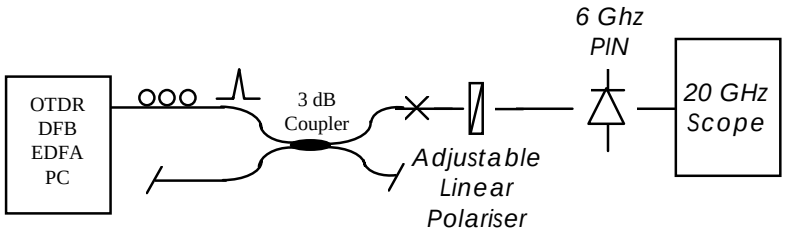

Figure 7.10 Set-up used for measuring the DOP and time consistency of output pulse from the enhanced OTDR.

Figure 7.11 (a) and (b) further shows the consistency of the output pulse with time over a measurement period of 30 minutes, where it can be seen in (a) and (b), that the pulse shape does not change noticeably whereas there is some small change of SOP over that time period. This time period is comparable to the measurement time needed in Section 7.3 for evaluating the SOP from the backscattered power using the single-channel polarimeter. At lower DOPs, the change of SOP along the pulse, and also the change of the SOP over measurement time, will contribute to an error in the measured SOP of the backscattered light on the Poincaré sphere which could be reduced by using a polariser at the output path of the OTDR but at the cost of reduced DR.

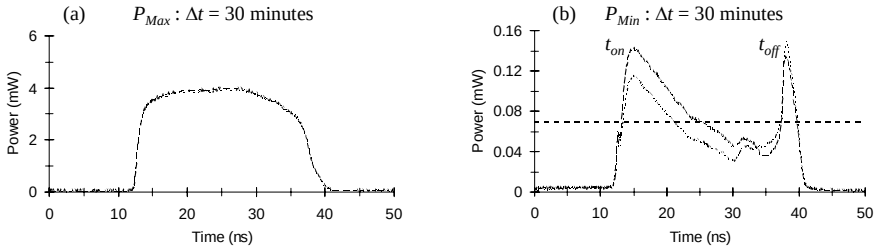

Figure 7.11 Measurement repeatability of the OTDR output pulse through polariser over a time period of 30 minutes. In (a) for maximum transmission and in (b) for minimum transmission.

7.2 A matrix and vector description of the backscattered SOP evolution in twisted fibres

In this section, the matrix description for the backscattered SOP evolution in twisted fibres will be derived, where the assumption made for the matrix description in forward direction (Subsection 5.1.1) will be assumed to be also true for counter propagating waves.

In single mode fibres, we assume negligible dichroism (no PDL) for the forward direction, uniform polarisation over the spatial mode field [55] and preservation of polarisation orthogonality at all points along the fibre[42]. In Section 4.5, it has been shown that the fibre behaves like a reciprocal medium and the assumptions for forward propagating waves can be taken as valid for counterpropagating waves. This we would also expect from theory, so long as the system behaves like a linear system (no Brillouin or Raman scattering), and in the absence of any nonreciprocal effects (Section 2.4) like the Faraday effect.

A more severe assumption is concerned with the scattering process in the fibre itself where ideal scattering in the derived model will be assumed. Ideal scattering, in this sense, we define as scattering from a short pulse so that the SOP does not change significantly within the pulsewidth (Section 7.5), so that there is no interference from the scattering points along the fibre. Further the scatter points in the fibre are ideal isotropic scatterers (Subsection 2.5.3) so that the scatter centre preserves the SOP (no phase or amplitude change). Under these assumptions the scattering process can be described by a reflection from an ideal mirror (Section 4.5) in describing the backscattered SOP evolution in an optical fibre.

The last assumption will be reconsidered in Section 7.5 because the measurement results obtained with POTDR showed that the measured fibres did not behave as we would expect from an ideal rotation matrix with ideal reflection which would preserve the DOP.

For ideal scattering and a linear reciprocal system, the magnitude of the Stokes vector is constrained to unity length, and the backscatter matrix in a fibre with uniform linear and circular birefringence can be obtained by extending the derived solution in Chapter 5 by including the reflection matrix $\mathbf{R}_M$ which changes the handedness of the scattered SOP.

7.2.1 A Mueller matrix description for backscattered light along fibres with and without twist

In Subsection 5.1.2, it was shown that the SOP evolution along the length l of a fibre with uniform linear birefringence $\delta\beta_L$, subject to a twist of γ, can be described by a local birefringence vector $\delta\vec{\beta}_F = \begin{pmatrix} \delta\beta_L & 0 & g\gamma - 2\gamma \end{pmatrix}^T$ followed by a rotation between the laboratory frame and fibre axes following the twist (Equation 5.31). Back reflection by ideal Rayleigh scattering induces an inversion of handedness which can be described by the mirror matrix $\mathbf{R}_M$ given in Equation 2.21, and the backward matrix is the transpose of the forward rotation matrix**.** The backscattered SOP, $\bar{\mathbf{s}}(l)$, observed at the input end of the fibre from the backscattered signal at the length l, along a uniformly twisted fibre, as shown in Figure 7.12, can be written as a rotation-reflection-rotation matrix as [15], [170], [171]

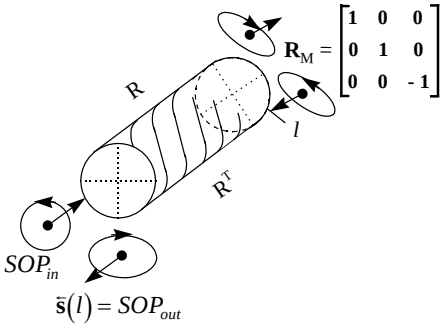

Figure 7.12 Simple fibre model for POTDR action with one backreflection point

$$\bar{\mathbf{s}}(l) = \mathbf{R}^T(\delta\vec{\beta}_F l)\mathbf{R}_z^T(2\gamma l)\mathbf{R}_M\mathbf{R}_z(2\gamma l)\mathbf{R}(\delta\vec{\beta}_F l)\bar{\mathbf{s}}(0) \tag{7.5}$$

The order of $\mathbf{R}_M$ and $\mathbf{R}_z$ can be exchanged because the reflection does not change with the rotation around the z-axis. The two matrices commute and the rotation with twist in Equation (7.5) cancels, which shows that the SOP evolution in the lab frame is the same as in the rotating frame for the backscattered SOP along the fibre

$$\bar{\mathbf{s}}(l) = \mathbf{R}^T(\delta\vec{\beta}_F l)\mathbf{R}_M\mathbf{R}(\delta\vec{\beta}_F l)\bar{\mathbf{s}}(0) \tag{7.6}$$

Equation (7.6) can be re-written as a rotation-reflection matrix [15], [171]

$$\bar{\mathbf{s}}(l) = \mathbf{R}_M\mathbf{R}(\delta\overleftarrow{\beta}_B l)\mathbf{R}(\delta\vec{\beta}_F l)\bar{\mathbf{s}}(0) = \mathbf{R}_M\mathbf{M}\bar{\mathbf{s}}(0) \tag{7.7}$$

where $\delta\overleftarrow{\beta}_B = \begin{pmatrix} \delta\beta_L & 0 & 2\gamma - g\gamma \end{pmatrix}^T$ is now the new rotation vector for the backward direction with opposite twist to the forward direction. Equation (7.7) can be understood in the following way: light travelling in the backward direction sees opposite twist to light travelling in the forward direction whereas the linear birefringence appears to be unchanged upon path reversal (Section 6.2). The frame of reference has been changed at the point of reflection (the

SOP remaining unchanged at reflection), and in order to be consistent with the frame of reference used in Equation (7.6), which is consistent with the principle of reciprocity (Section 2.4), the resultant rotation matrix **M** has been multiplied by the mirror matrix to obtain the inverted handedness of the output SOP.

In analysing the polarisation OTDR traces as will be carried out in the following sections, the inversion of the handedness of the output SOP will be unimportant because only the relative handedness of the output SOP will be measured. Equation (7.7) can be visualised on the Poincaré sphere, as shown in Figure 7.13(a), as two consecutive rotations around the two rotation vectors $\delta\vec{\beta}_F$ and $\delta\overleftarrow{\beta}_B$. In Figure 7.13 (b) to (d), the backscattered SOP evolution has been plotted on the Poincaré sphere using Equation (7.7) for the case of zero twist in (a) and in (c) and (d) for $\gamma/\delta\beta_L$ = 0.25π and 0.5π respectively. The periodicity and the shape of the backscattered SOP evolution on the Poincaré sphere is considered next which will be useful in analysing POTDR traces in order to obtain information of the linear and circular birefringence in the fibre, and from that the DGD may be estimated using Equation 5.45.

7.2.2 The periodicity of the backscattered SOP evolution

For only linear birefringence, the vector in the forward and backward direction points in the same direction, $\delta\vec{\beta}_F = \delta\overleftarrow{\beta}_B$, and the backscattered SOP, traces just a circle on the Poincaré sphere (Figure 7.13(b)) around the resultant vector $\delta\vec{\beta}_{F,B} = 2\delta\vec{\beta}_F$. For backscattering, the trace of the SOP evolution as a function of length *l* rotates with double the speed compared to just the forward direction, and the periodicity *L* for the backscattered trace is given by

$$L = \pi/\delta\beta_L \tag{7.8}$$

The periodicity given in Equation (7.8) is half the beat length L_b of the two polarisation modes as defined in Equation 3.17 for the forward direction. For circular birefringence only, the vectors are opposite to each other and the net rotation for the backscatter is zero. The SOP is fixed along the fibre and just changes its handedness relative to the input SOP. Birefringence measurements using POTDR often assume that the linear birefringence is the dominant birefringence in the fibre, such that the twist induced circular birefringence can be ignored, and allowing the polarisation dispersion to be inferred from the periodicity of the POTDR trace as determined in Equation (7.8). However, in a real fibre (cable), twist can hardly be avoided (Subsection 6.1.2.2) and even a small amount of twist will have a

considerable influence on the POTDR output (see Figure 7.13 (b) and (c)) and can lead to an overestimation of the fibres birefringence and DGD if it is neglected [15], [171].

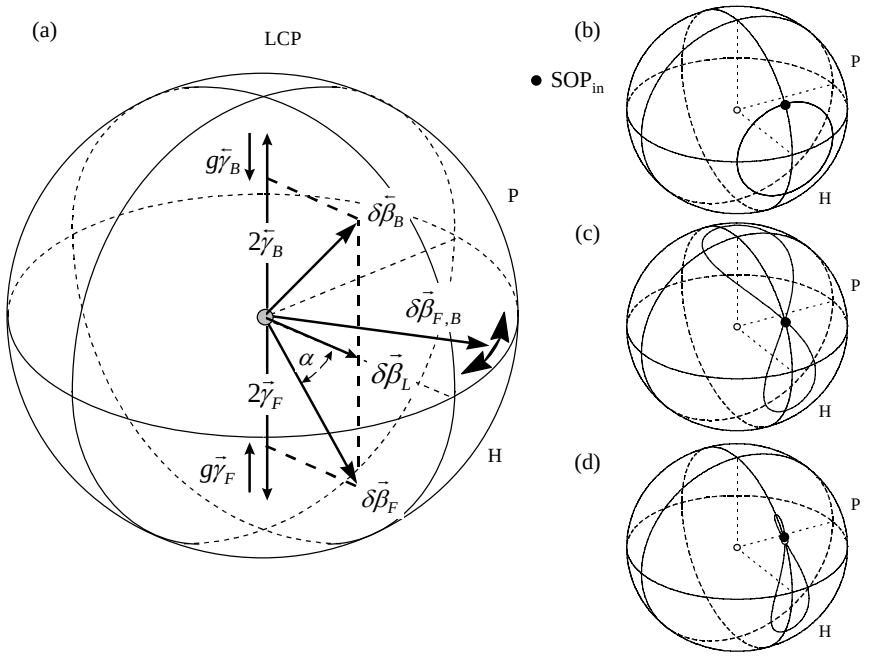

Figure 7.13 (a) Resultant birefringence vectors for forward and backscattered light in rotating reference frame. (b-d) Simulation of SOP evolution of backscattered light at launch end face for $\gamma/\delta\beta_L$ = 0, 0.25π and 0.5π respectively, the input SOP is [cos(π/6), 0, sin((π/6)].

For uniform linear and circular birefringence, the shape formed by the locus of the output SOP will generally have an elliptical form but may intersect itself in a "figure of eight" manner, depending on $\delta\beta_L$, γ and the input SOP (Figure 7.13 (b) and (c)). The locus of the backscattered SOP, as a function of *l*, will always complete an integral number of closed loops on the Poincaré sphere if the rotation angle $\delta\beta = \sqrt{\delta\beta_L^2 + (2\gamma - g\gamma)^2}$ around the vector $\delta\vec{\beta}_F$ and $\delta\overleftarrow{\beta}_B$ is a multiple of 2π and, hence, in general, the periodicity *L* of the POTDR trace is given by

$$L = 2\pi/\delta\beta \tag{7.9}$$

The intersection point of the figure-of-eight SOP locus (Figure 7.13(b)) occurs whenever the rotation angle $\delta\beta$ is equal to $\pi + N2\pi$ where N = 0, 1, 2 … In Appendix B (Figure B.8) the backscattered SOP evolution for different input SOP has been plotted for increasing twist, showing the progression of the backscattered SOP locus on the Poincaré sphere. The angle α

between the resultant vector $\delta\vec{\beta}_F$ and the equatorial plane (or $\delta\overleftarrow{\beta}_B$) as indicated in Figure 7.13(a), determines (for a fixed input SOP) the shape of the SOP evolution on the Poincaré sphere and is given by

$$\tan(\alpha) = \frac{(2\gamma - g\gamma)}{\delta\beta_L} \tag{7.10}$$

From Equation (7.9) and (7.10), it may be seen that if the periodicity L and angle α of the resultant vector in forward or backward direction are known (or in other words the shape of the SOP evolution on the Poincaré sphere), then the magnitude of the linear birefringence and the twist of a fibre may be estimated from the backscattered SOP evolution using POTDR.

7.2.3 The response of an analyser

The dual occurrence of the rotation matrix **R** in Equation (7.7) indicates that the matrix coefficients of **M** are quadratic in $\cos(\delta\beta \bullet l)$ and $\sin(\delta\beta \bullet l)$ (see Equation 5.30), and in general, the intensity through an analyser (Section 4.2) may be expressed in the form of a Fourier series [15]

$$\begin{aligned} I &= a_0 + \sum_{n=1}^{2} a_n \cos(n\delta\beta l) + b_n \sin(n\delta\beta l) \\ &= a_0 + \sum_{n=1}^{2} a_n \cos(2\pi\kappa_n l) + b_n \sin(2\pi\kappa_n l) \end{aligned} \tag{7.11}$$

where the magnitudes of the coefficients a and b depends on the linear and circular birefringence, and the input SOP and $\kappa_{1,2}$ are the spatial frequencies in cycles/m. For the simple case of zero twist, the SOP traces just a circle (Figure 7.13(b)) as discussed above, a_1 and b_1 being zero, leading to just one component in the POTDR power spectrum, as expected from Equation (7.8). For backreflection from a section with twist, a_1 and b_1 are now not zero which, together with a_2 and b_2, lead to two components in the POTDR spectrum, which may be called the fundamental and second harmonic fluctuations. This qualitative difference between the two POTDR spectra makes it, in general, possible to detect sections of fibre with twist and no twist for an arbitrary input SOP and fixed analyser position, as will be shown in Section 7.3, where the limitations in analysing POTDR output data using this method will also be discussed.

7.2.4 A vector description for backscattered light along fibres with and without twist

In Figure 7.13(a), the rotation around the two vectors, $\delta\vec{\beta}_F$ and $\delta\vec{\beta}_B$, can be replaced by a single equivalent rotation [217] around the vector $\delta\vec{\beta}_{F,B}$ given by [171]

$$\tan\left(\delta\beta_{F,B}/2\right)\delta\hat{\beta}_{F,B} = \tan\left(\delta\beta l/2\right)\frac{\delta\hat{\beta}_F + \delta\hat{\beta}_B + \tan\left(\delta\beta l/2\right)\delta\hat{\beta}_B \times \delta\hat{\beta}_F}{1-\tan^2\left(\delta\beta l/2\right)\delta\hat{\beta}_F\delta\hat{\beta}_B} \quad (7.12)$$

with the rotation angle $\delta\beta_{F,B}$ as $\tan\left(\delta\beta_{F,B}/2\right) = \dfrac{2b\dfrac{\delta\beta_L}{\delta\beta}\tan\left(\dfrac{\delta\beta}{2}l\right)}{1-\dfrac{\delta\beta_L^2-\left(2\gamma-\delta\beta_C\right)^2}{\delta\beta^2}\tan^2\left(\dfrac{\delta\beta}{2}l\right)}$ and the rotation axis $\delta\hat{\beta}_{F,B} = \dfrac{1}{b}\begin{bmatrix}1\\ \dfrac{\delta\beta_C-2\gamma}{\delta\beta}\tan\left(\dfrac{\delta\beta}{2}l\right)\\ 0\end{bmatrix}$ where $b = \sqrt{1+\dfrac{\tan^2\left(\dfrac{\delta\beta}{2}l\right)\left(2\gamma-\delta\beta_C\right)^2}{\delta\beta^2}}$.

Equation (7.12) gives a very useful form for implementation in a computing algorithm to analyse the backscatter traces of POTDR, as will be used in Section 7.3 and 7.4. The rotation axis of the resultant rotation in Equation (7.12) lies in the equatorial plane (see also Figure 7.13(a)), proving that for a reciprocal system in the presence of twist, the eigenvectors for one round trip are linearly polarised, as shown in Section 4.5 for different optical elements. However, although the circular birefringence cancels for one round trip and the fibre may look, with respect to one backreflection point, as if it possesed just linear birefringence, the presence of twist can still be observed with respect to a second backreflection point because the direction and angle of rotation of $\delta\vec{\beta}_{F,B}$ depends on the fibre twist. This would also be expected because twist not only induces circular birefringence, but also reduces the effective linear birefringence as shown in Figure 5.9. POTDR fluctuation is, in general, strongly influenced by twist, as will be shown, but to differentiate between the two kinds of twist, i.e. whether elastic twist or frozen in twist as in spun fibres, would be difficult from the POTDR trace without prior knowledge of the kind of twist expected, due to the small effect of the rotation coefficient (gγ compared to 2γ, g ≈ 0.14) in the resultant birefringence vector $\delta\beta$ in Equation (7.12).

7.3 Measurement results and analysis from the single-channel POTDR on fibres with different twist rates

In this section, the POTDR measurement results on fibres with and without twist are shown. The majority of the early results have been taken using the single-channel POTDR with DFB laser which showed the type of results predicted from theory. Since the first reported results, improvement of the measurement set-up, by using a fibre polariser at the output of the single-channel polarimeter, and also by using a novel four-channel POTDR, has been obtained reducing the error in the measured SOP (Section 7.4 and Appendix B, Figure B.6).

In the presence of twist the backscattered SOP evolution can be characterised by the periodicity of the SOP evolution (Equation (7.9)) and by the shape of the SOP evolution if plotted on the Poincaré sphere (Equation (7.10)). For the single-channel POTDR, the error in the periodicity of the SOP evolution is determined by the two-point resolution, which is ~±3 metres (Subsection 7.1.4.4), and the error in the shape of the SOP evolution, which will be treated in Section 7.5, may be taken as ±3.6° in the average overall SOP. For zero twist, the error of ±3 metres, due to the two-point resolution, is determined by the periodicity of the SOP evolution as given in Equation (7.8).

7.3.1 Measurement conditions

The experimental results using POTDR were carried out on some of the freely suspended fibres described in Chapter 6 for measuring the DGD. Measuring the DGD versus twist allowed, not only the determination of the zero twist in the fibre experimentally, but also a comparison with the estimated DPD value obtained from the measured birefringence values using POTDR. The measured and analysed fibres, using POTDR, are S-SMF 2, S-SMF 3, DSF 1 and DSF 3 (see Table 6.1 in Chapter 6). In Section 7.4, there will also be a POTDR measurement of S-SMF 2 made on the shipping bobbin.

7.3.2 Fluctuation at different twist rates with power spectrum

Figure 7.14 shows the POTDR power fluctuations measured on S-SMF 3 for increasing twist rates (twisted at the far end) at two different analyser positions but fixed input SOP. The POTDR power fluctuation has been sampled every 1 metre and the fluctuation is normalised to the highest peak value. At zero twist, in Figure 7.14 (a) and (b), the POTDR fluctuation shows a single frequency as would be expected from Equation (7.11), with a_1 and b_1 equal to zero, whereas for the twisted fibre more than one frequency can be observed in the fluctuation which is investigated next.

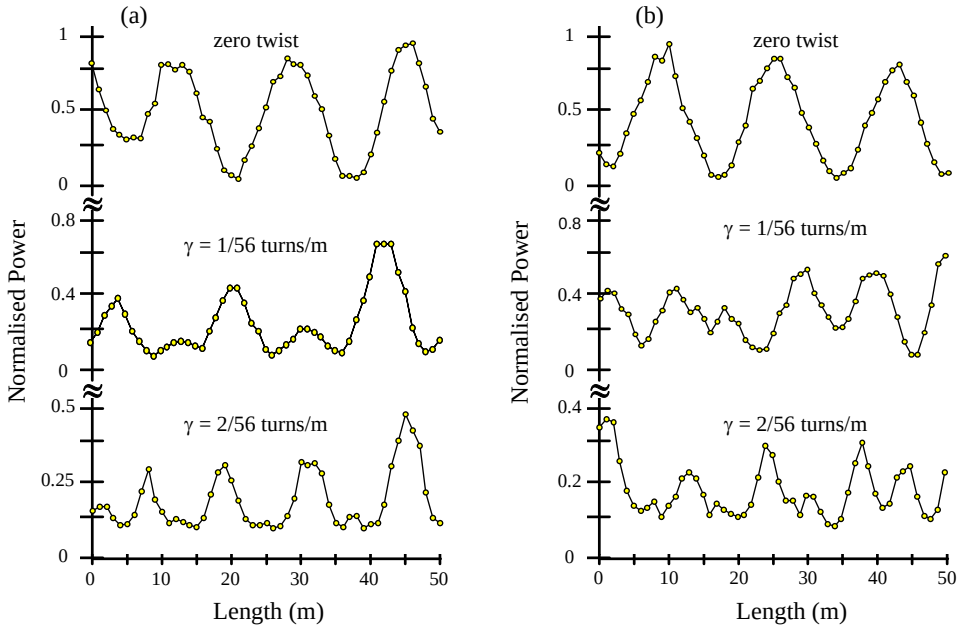

Figure 7.14 Measured data points of the normalised output power of POTDR trace versus length, S-SMF 3 twisted at far end. In (a) and (b) for two different analyser positions but fixed input SOP.

Figure 7.15 shows the normalised power spectra of the measured POTDR fluctuation as shown in Figure 7.14 for the fibre with and without twist. To obtain the power spectrum, the DC value (a_0) has been subtracted from the fluctuation and an FFT has been applied with a Hamming window. At zero twist, the frequency spectrum shows just one component for the two analyser positions. The peak value is at κ_2 = 0.0625 cycles/m giving a linear birefringence of $\delta\beta_L \approx 0.2$ rad/m (Equation (7.8)). The error in $\delta\beta_L$, determined from the waveform periodicity, is mainly given by the two-point resolution of ~3 metres and may be taken as ±20%.

From the measured linear birefringence for S-SMF 3, the differential phase delay (DPD) (at λ = 1.55 μm) using Equation 3.19 gives a value of DPD ≈ 0.16 ps/km. The relative difference Δ_τ in the DPD and the measured DGD from S-SMF 3 (given in Table 6.1 as 0.29 ps/km around the centre frequency of 1.55 μm) is $\Delta_\tau \approx 50\%$. This difference in the DGD and DPD is in the range predicted by Figure 3.15(b) for S-SMFs with slight variations in their fibre parameters. The offset predicted is between 40% and 60% at 1.55 μm.

On applying twist, the POTDR power spectrum acquires a second component due to the non-zero value of a_1 and b_1 as expected from Equation (7.11), which leads to the beating observed in Figure 7.14. The spatial frequencies, κ_1 and κ_2, of the twisted fibre are 0.047 and 0.094 cycles/m at γ = 1/56 turns/m and 0.078 and 0.156 at γ = 2/56 turns/m. Figure 7.16 shows the good agreement of the measured and calculated spatial frequencies for S-SMF 3 using Equation (7.11) with $\delta\beta_L$ = 0.2 rad/m, as a function of twist. From Figure 7.16, it can be seen that even a small amount of twist at low linear birefringence values can cause high spatial frequencies in the backscatter trace of the POTDR fluctuation, which in order to be resolved, can put some tough requirements on the necessary pulsewidth and bandwidth of a POTDR if used to measure real fibres where twist is often unavoidable.

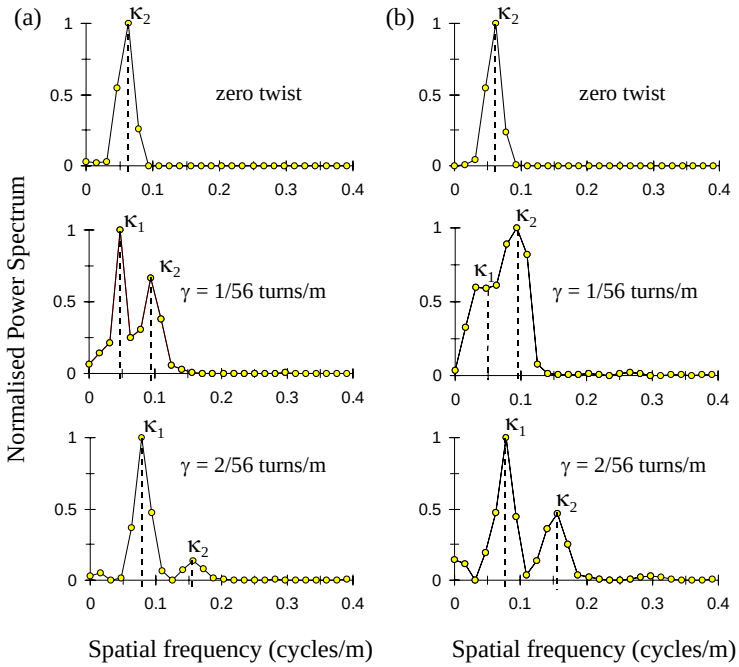

Figure 7.15 Normalised power spectrum from POTDR fluctuation as shown in Figure 7.14

Theoretically, it would be sufficient to use just two different analyser positions (rotating the angle of the retarder or the angle of the polariser axis), or two different input SOPs, to see a change in the amplitudes of the two frequencies as shown in Figure 7.15. But a more accurate estimation of the fibre birefringence (and confirmation of the presence of twist) can be made if more input SOPs and analyser positions are used, because one of the amplitudes of the two frequencies may be preferred for the majority of possible input SOPs and analyser positions, depending on the amount of twist in the fibre. Using the above procedure, it is therefore possible to identify sections of a fibre without twist which would allow estimation of the fibre DPD (DGD). Such a POTDR could be simply realised by adding a polariser (e.g. fibre polariser) in the receiver path of an OTDR and randomly varying the input SOP for each measurement with, for example, a fibre polarisation controller.

Although the idea of using a single polariser is very appealing because of its simplicity and cheapness by adapting to a commercial OTDR, unfortunately, there are also some drawbacks with this technique. One problem as seen in Figure 7.15 is at low twist rates. The spectral resolution in the power spectrum which, if too low due to not enough periods in the fluctuation, can lead to difficulties in separating the peaks. At least one period in the fluctuation would be required to obtain a useful power spectrum. Another problem is that although it is possible to detect fibre sections with twist using a single polariser to modify an OTDR, it is not possible from the sections with twist to deduce the magnitude of the linear birefringence and twist (without prior knowledge of $\delta\beta_L$) because there are two unknowns in Equation (7.9). Moreover, the SOP measurement approach is more robust against power fluctuation in the backscatter trace as it may be caused by changing attenuation, reflection from splice points or due to coherent noise, because the SOP is specified for individual backscatter points along the fibre within the POTDR resolution.

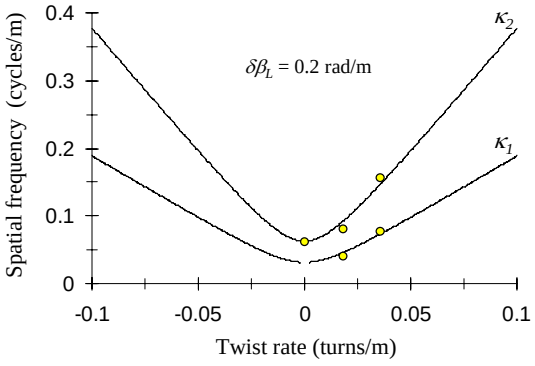

Figure 7.16 Measured and calculated spatial frequencies against twist from POTDR fluctuation of S-SMF 3.

7.3.3 Backscattered SOP evolution at different twist rates

By analysing the complete SOP evolution of the backscattered light along the fibre, the magnitude of the twist and linear birefringence in the fibre can be determined from the

periodicity of the backscattered SOP evolution (Equation (7.9)), and by using the additional information of the shape of the SOP evolution on the Poincaré sphere (Equation (7.10)), as will be shown next.

Equation (7.7) may be extended to include the SOP evolution as measured with the POTDR set-up, shown in Figure 7.17, by multiplying the backscattered SOP, $\vec{\mathbf{s}}(l)$, with a constant rotation matrix, $\mathbf{R}_C$ which is the transmission matrix of the 3 dB coupler in the backward direction, so that [15]

$$\vec{\mathbf{s}}(l) = \mathbf{R}_C \mathbf{R}_M \mathbf{M}(\delta\vec{\beta} l)\vec{\mathbf{s}}(0) \tag{7.13}$$

$\mathbf{R}_C$ is just an overall rotation of the backscattered SOP trace on the Poincaré sphere which does not change the trace of the SOP evolution on the Poincaré sphere. Figure 7.18 shows the measured and best fit simulation results at different twist rates for the backscattered SOP from S-SMF 3. The simulation is fitted to the measurements interactively on both the Poincaré sphere and on the azimuth - ellipticity variation of the SOP as a direct function of length using Equation (7.13). In principle, by searching for the best fit in this way, Equations (7.9) and (7.10) are now fulfilled, allowing the unique determination of the magnitude of linear and circular birefringence in the fibre. However, the absolute direction of the twist (left or right handed) cannot be determined because of the unknown rotation of $\mathbf{R}_C$.

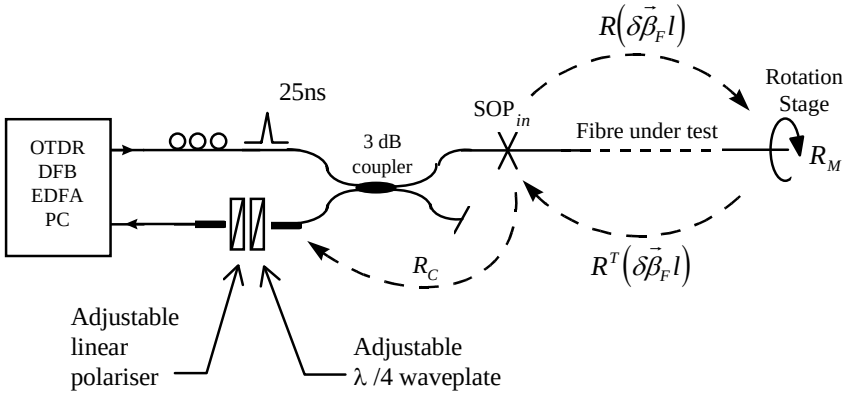

Figure 7.17 Single-channel polarimetric OTDR set-up.

Figure 7.18(a) shows the SOP evolution on the Poincaré sphere for the fibre in the zero twist condition, defined as that giving maximum DGD (see Section 6.2).

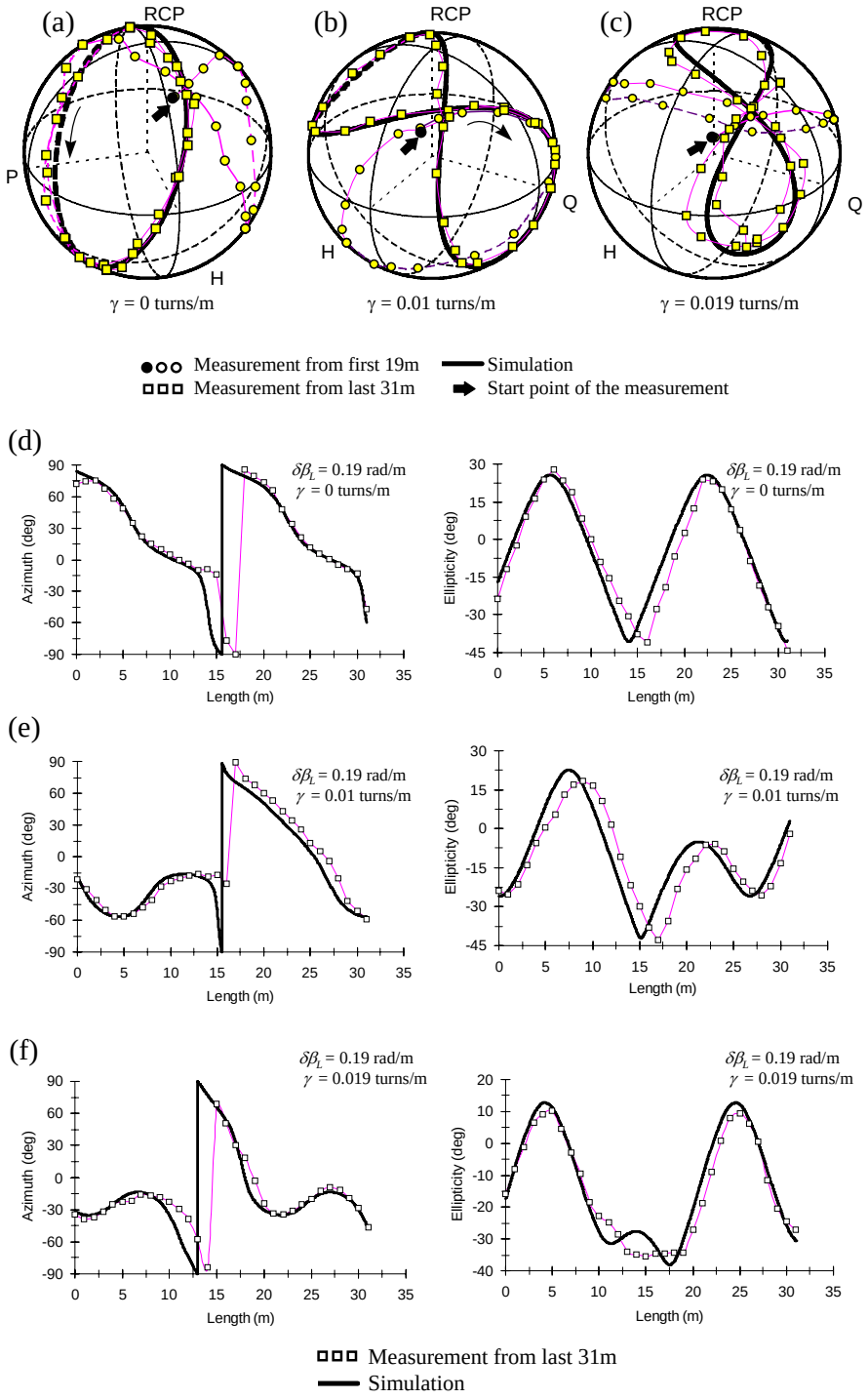

Figure 7.18 Measurement and simulation of the SOP evolution along S-SMF 3 with different twist rates using the single-channel POTDR.

Now if the zero twist condition actually existed over the whole length of the fibre, then the SOP trace would just be a repeated circle. However, in the data of Figure 7.18(a), only the last 31 metres of the fibre shows a repeated circular trace on the Poincaré sphere, the first 19

metres giving data points away from the circle. From this, and measuring the fibre with left and right hand twist using the POTDR (see Subsection 7.3.6), it could be concluded that the fibre possesses some small non-uniform twist which may be frozen in during the fibre fabrication process (the small non-uniform twist in the first 19 metres of fibre has been found to be < 0.2/56 turns/m).

The last 31 metres of fibre was then modelled as a section with zero twist and constant linear birefringence as the variable to find the best fit to the measurement by using Equation (7.13). The best fit simulation, indicated in Figure 7.18 (a) and (d), was obtained for $\delta\beta_L$ = 0.19 rad/m for the last 31 metres of fibre, which is within 5% of the value estimated from the power spectrum for the total 50 metre fibre length in Figure 7.15(a), and is within the error expected for the POTDR resolution. In applying a twist of 0.01 turns/m, Figure 7.18 (b) and (e), the backscattered SOP of the last 31 metres of fibre traces a figure of eight shape in accordance with Equation (7.12). For the higher applied twist rate of 0.019 turns/m, Figure 7.18 (c) and (f), the area of the figure eight decreases as predicted in Figure 7.13 (c) to (d) by using Equation (7.12). The simulation traces for these two twist values, Figure 7.18 (b) and (e) and Figure 7.18 (c) and (f), again give $\delta\beta_L$ = 0.19 rad/m and twist values of 0.012 and 0.021 turns/m respectively for the best fit. The error in the twist estimated with POTDR is < 20% for the two mechanically applied twist rates.

7.3.4 The DOP of the backscattered SOP evolution

Figure 7.19 shows the DOP of the backscattered SOP from Figure 7.18 over the full length of the fibre. The average DOP at zero twist and with twist are close to 80%, which explains why the largest peak to peak value in the observed POTDR fluctuation shows just an extinction ratio of up to 10 dB (see Figure 7.5). The DOP shows also some fluctuation of about ±10% around its average value along the fibre.

The fluctuation which shows a spatial frequency related to the fibre birefringence (~0.06 cycles/m) may be explained from the simulation results as obtained in Section 4.4 (e.g. Figure 4.8), which shows a dependence of the measured DOP on the SOP in the presence of noise and error in the analysing optics. This argument has been strengthened by carrying out measurements with different input SOPs, for a backscattered SOP evolution with less SOP variation as shown in the next subsection, and then the fluctuation in the DOP is smaller. The lower average DOP in the backscattered signal may be partially explained by the DOP of the incident pulse (~94%), the noise present in the measured trace and due to the spatial extent of the pulse. We have also performed measurements with a polariser at the output of the POTDR

(Setion 7.4 and Appendix B), which ensures that the injected pulse into the fibre is ~100% polarised, and the backscattered DOP nevertheless showed an average DOP of around 80%. It is interesting that this 80% DOP has also been reported in Reference [197] using a polarimetric OTDR, although this was measured at $\lambda \sim 0.5$ μm. This lower DOP, we could conclude, may be inherent to some degree (more or less depending on the noise and error in the used system) in the fibre scattering process itself which has been assumed ideal in the theory, but needs further investigation. In general, a lower DOP is not desired as it increases the error in the measured SOP in the presence of noise as discussed in Section 4.4.

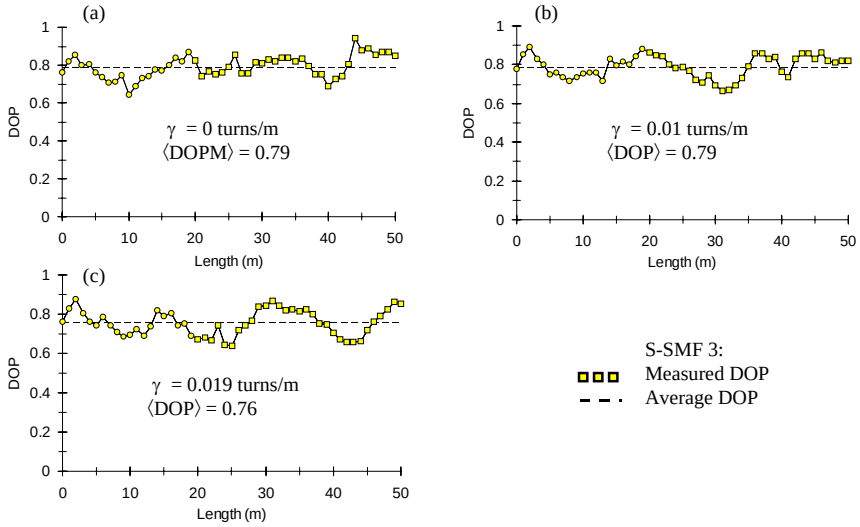

Figure 7.19 The DOP of the backscattered SOP as shown in Figure 7.18 for the different twist rates.

7.3.5 Backscattered SOP evolution with different input SOP

Figure 7.20 (a) to (d) shows the SOP evolution and DOP for S-SMF 3 at zero twist for a different input SOP. The SOP evolution on the Poincaré sphere traces a small circle indicating that the input SOP is close to one of the PEMs of the fibre. From the periodicity of the azimuth -ellipticity as indicated in Figure 7.20 (a) and (b), the linear birefringence of the fibre has been estimated as 0.19 rad/m, which as expected, agrees with the linear birefringence estimated from Figure 7.18 (d), where the backscattered SOP evolution showed a great circle on the Poincaré sphere. The DOP in Figure 7.20 (b) shows a slightly higher value and a fluctuation with less magnitude compared to the DOP in Figure 7.19(a), which for the fluctuation, as mentioned in Subsection 7.3.4, is most probably due to the dependence of the DOP on the actual SOP.

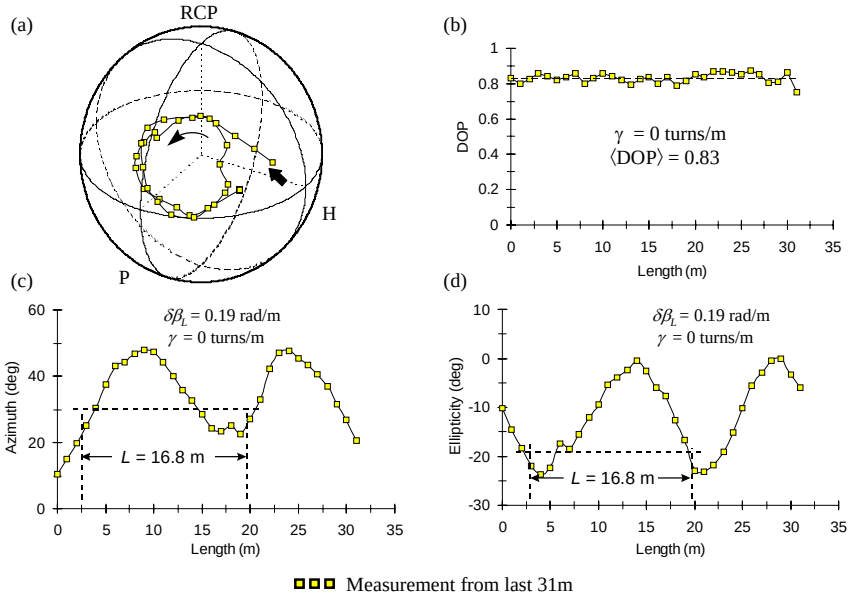

Figure 7.20 Measurement of the backscattered SOP evolution at zero twist along S-SMF 3 with input SOP close to one of the PEMs of the fibre.

7.3.6 Backscatter results for left and right hand twist

Figure 7.21 shows the backscattered SOP evolution measured along S-SMF 3 for clockwise (cw) and counter clockwise (ccw) twist, showing the area of the figure eight decreasing symmetrically about the zero twist position as expected from the theory. Comparing carefully the traces of the backscattered SOP evolution with cw (Figure 7.21 (a-c)) and ccw twist (Figure 7.21 (d-f)) with each other, it can be seen that for the cw twist, the area of the eight seems to get smaller with distance along the fibre, whereas for the ccw twist it seems to be vice versa. This supports the assumption in Subsection 7.3.3 that S-SMF 3 contains some permanent twist, although it could be argued that the elastic twist applied at the far end of the fibre did not evolve uniformly through the fibre. We have carried out a visible check to ensure the uniformity of the twist throughout the fibre.

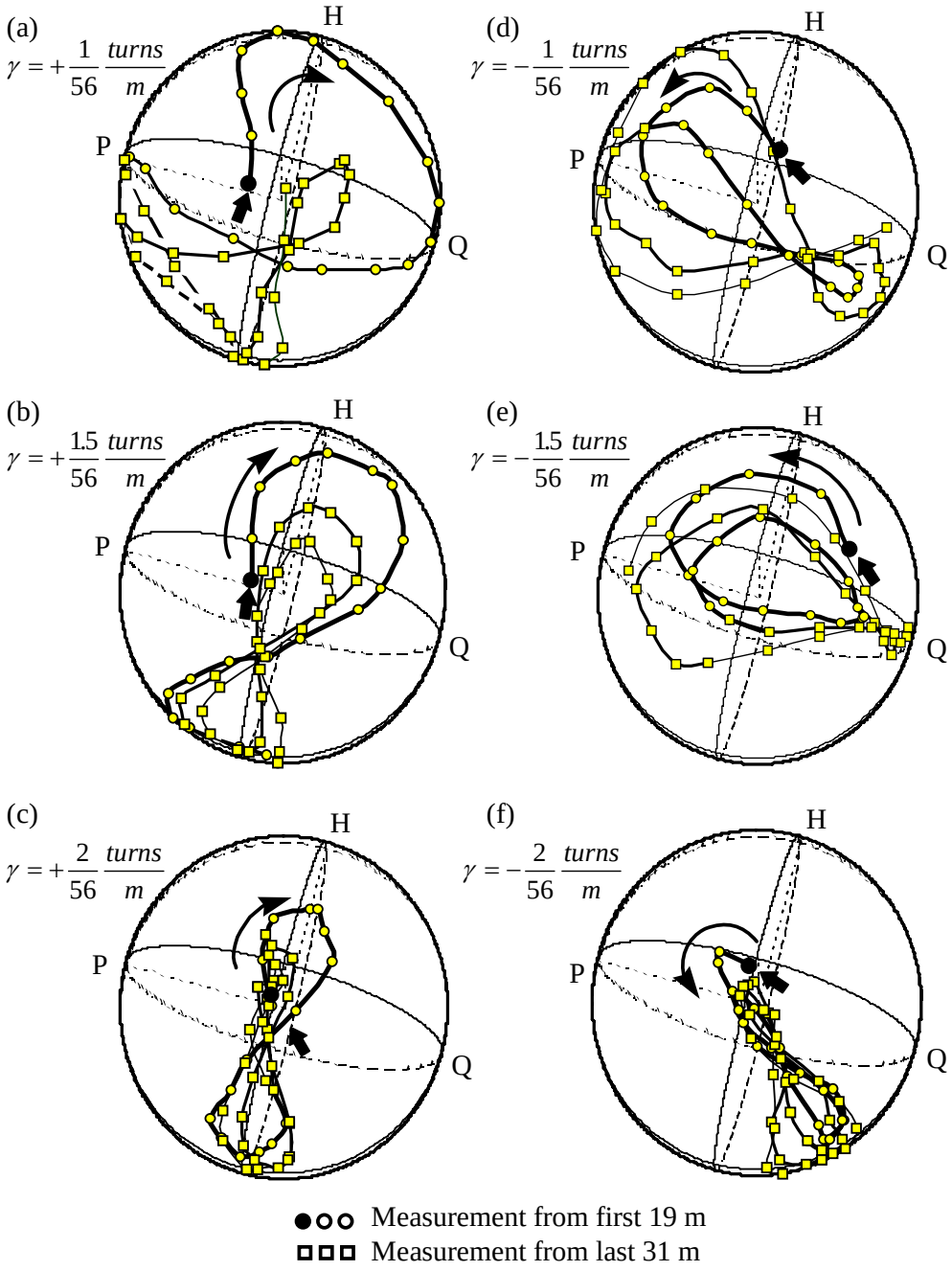

Figure 7.21 Measurement of the backscattered SOP evolution along S-SMF 3 with clockwise and counter clockwise twist. On the right hand side (a) to (c) with cw twist and on the hand left side (d) to (f) with ccw twist.

7.4 A novel four-channel POTDR and its measurement results on different fibres

7.4.1 The four-channel polarimetric OTDR

The four-channel polarimetric OTDR developed at the University of Essex is a high speed form of the Essex polarimeter (see Section 4.3). The development of the four-channel polarimetric OTDR, as shown in Figure 7.22, was carried out by PhD student, John Ellison, at the University of Essex. The four-channel polarimetric OTDR has a ~1 metre resolution and a 14 dB dynamic range per channel (after 80 averages) for a 10 ns pulsewidth, which allowed the measurement and analysis of fibres with higher birefringence values like DSF 3 [214], [215].

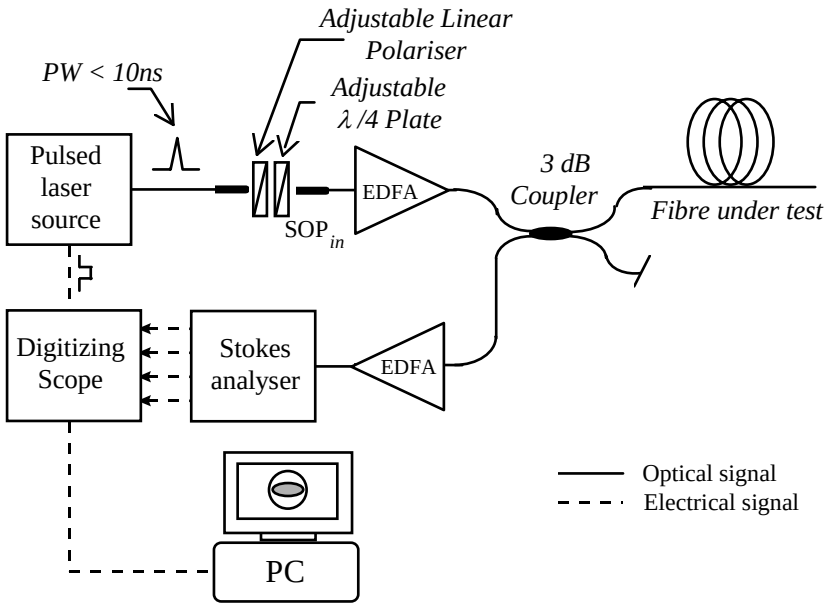

Figure 7.22 Four-channel Stokes OTDR set-up with fibre under test

The set-up of the Polarimetric OTDR is shown schematically in Figure 7.22. High peak power pulses (23 dBm, <10 ns) of known sets of states of polarisation (SOP) are launched into the fibre. The Rayleigh backscatter is optically amplified by a low noise EDFA, split into the four Stokes components and sent to four high sensitivity, 1.5 GHz bandwidth receivers. The two-point resolution is ~ 1 m (Equation (7.4)) for the 10 ns pulse and the averaging is performed on a 4 channel digitizing oscilloscope. In order to reduce noise in the POTDR data, a digital filter with a cut-off frequency at about 200 MHz (corresponding to a spatial resolution of ~1 metre) has been applied to the measured data which increased the SNR to about 20 dB. The measurement time for one set of measurement results (for one input SOP) is about 1.5

minutes, including averaging and data transfer to the computer. This is about 20 times faster than the single-channel POTDR.

7.4.2 Measurement results on different fibres

7.4.2.1 Free-hanging fibre

Figure 7.23 (a) and (b) shows the measurement results obtained from the four-channel POTDR for S-SMF 2 and for DSF 3 hung in a catenary. S-SMF 2 in Figure 7.23 (a) shows a circle on the Poincaré sphere indicating zero twist with a linear birefringence of 0.18 ± 0.01 rad/m.

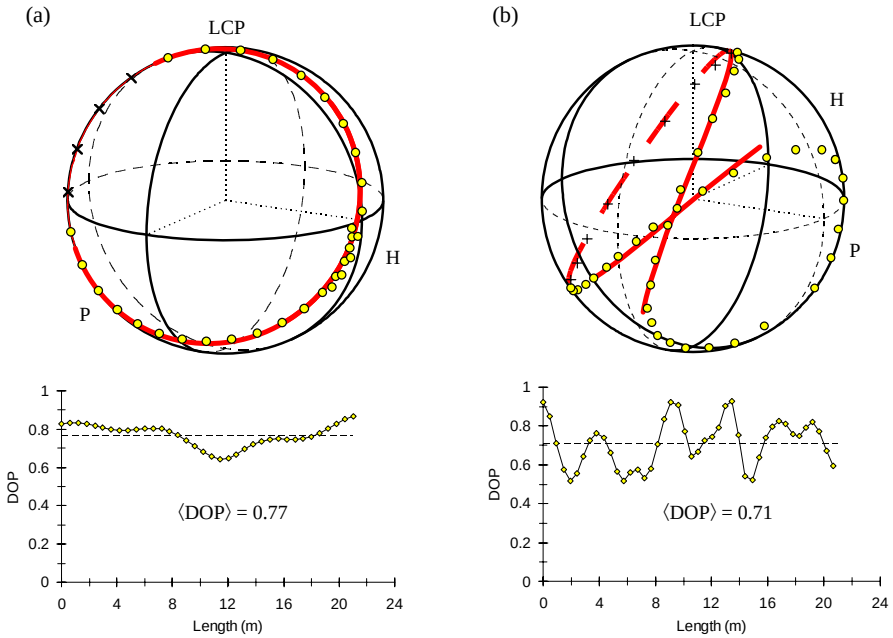

Figure 7.23 Measured and calculated SOP evolution using the four-channel polarimetric OTDR. In (a) for S-SMF 2 with DOP and in (b) for DSF 3 with DOP.

Figure 7.23 (b) also shows the backscattered SOP evolution for DSF 3 close to zero twist with the circle just to beginning to open out to the figure of eight shape expected from twisted fibres. The best fit simulation results using Equation (7.12) gives a linear birefringence of 0.67 rad/m with a twist of 0.015 turns/m. The error in the estimated linear birefringence and the twist from the best fit depend on both the two-point resolution and the overall error in the SOP evolution. However, because the twist is small, the error in the linear birefringence may be taken as defined by the two-point resolution of $\Delta z = \pm 1$ m (0.67 ± 0.15 rad/m), and the error in the twist can be estimated from the average error of the SOP evolution on the

Poincaré sphere ($\langle\varepsilon\rangle \approx 2.4°$, Section 7.5) and can be taken as below ±10% (0.015 ± 0.0015 turns/m).

Figure 7.23 (a) and (b) shows the DOP of the backscattered SOP evolution with average values of about 77% and 71% for the S-SMF and the DSF respectively. These DOP values, significantly lower than unity, cannot be fully explained by the measurement conditions. This is because the output pulse of the four-channel POTDR is fully polarised (~100%)[6], the SNR is ~ 20 dB, and the expected experimental error, from the error analysis in Section 4.4, Figure 4.7(b), should lead to an average measured DOP of ~99%. The main reason for the lower average DOP may be found in the scattering process itself. The fluctuation in the measured DOP which shows higher spatial frequencies for the DSF may be partly due to the measurement errors (see Figure 4.7(b)) because the higher birefringence, in general, causes the SOP to change faster with length, which is reflected in the higher spatial frequencies as observed in Figure 7.23(b) for DSF 3.

7.4.2.2 Fibre wound on fibre bobbin

The backscattered SOP has been measured for S-SMF 3 (different fibre section to that analysed in Section 7.3) which has been loosely spooled onto a standard shipping bobbin with diameter ~ 15 cm. Figure 7.24(a) shows the evolution of the Stokes parameters as a function of length. It can be seen that the Stokes parameters show a uniform sinusoidal behaviour over short sections, whereas over the whole length this is distorted due to some random perturbation caused by non-uniform twist and fibre kinks along the fibre.

Figure 7.24 (b) and (c) shows the SOP evolution with best fit for two sections of S-SMF 3 as indicated in Figure 7.24(a). On the Poincaré sphere, the SOP evolution along the whole fibre showed a repeating figure of eight pattern with the orientation of the figure of eight changing throughout the fibre due to the random fibre axes orientation. The figure of eight is distorted for fibre sections with non-uniform birefringence. The best fit curves of the two sections shown give linear birefringence and twist values of 0.31 rad/m and 0.018 turns/m for the first section (Figure 7.24 (b)), and 0.36 rad/m and 0.028 turns/m for the second section (Figure 7.24 (b)). The bend birefringence caused by spooling the fibre is $\delta\beta_L \approx 0.33$ rad/m (Equation 3.34 for $\lambda = 1.55$ μm) and the linear birefringence values as determined from POTDR are slightly above and below that value. This would also be expected because the net linear

[6] The DOP of the output pulse has been measured to be 100% with a uniform SOP over its entire length (Subsection 7.1.4.6). This has been achieved by using DFB laser with a polariser at the output path and further due to the use of low PDL and PMD isolators in the EDFA stages.

birefringence depends on the vectorial sum of the bend birefringence and the internal birefringence ($\delta\beta_L \approx 0.19$ rad/m) as discussed in Section 5.1.1, although in our case the measured difference is of the same magnitude as the expected measurement error. The average backscattered degree of polarisation of the whole fibre has been calculated as 77%.

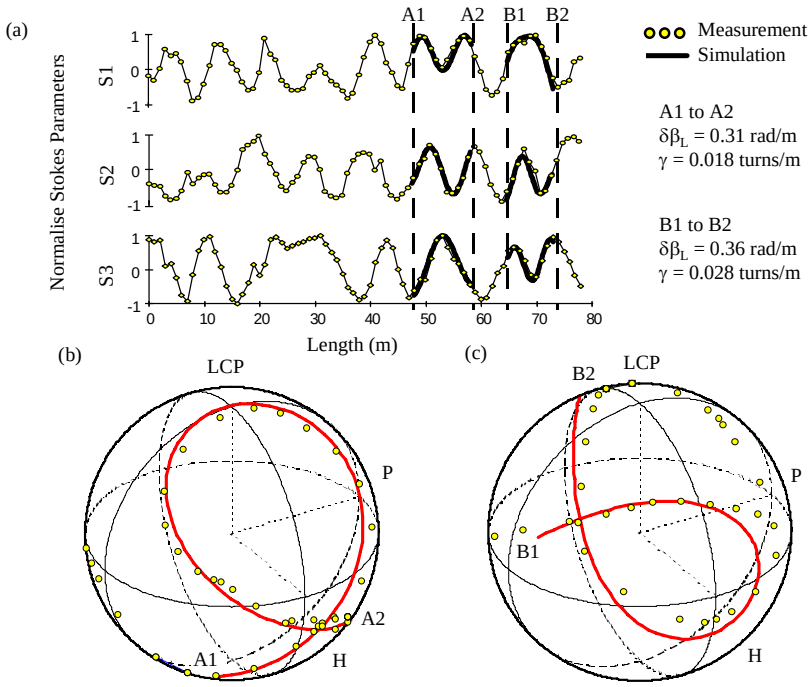

Figure 7.24 Measurement and calculated values for the backscattered SOP evolution along S-SMF 3 wound on fibre bobbin using the four-channel polarimetric OTDR. In (a) the normalised Stokes parameters as a function of length and in (b) and (c) the backscattered SOP evolution for two sections of the fibre.

Figure 7.25 shows the determinant of the analysed backscatter matrix as a function of length. The matrices have been calculated along the fibre from the measured backscattered SOPs and from nine known input SOPs which are generated by rotating the $\lambda/4$ plate in 20° steps. The average value of the determinant shows a value close to − 1 as would be expected for a rotation-reflection matrix. The fluctuation again indicates the error in the measurement and may also indicate the non-ideal scattering.

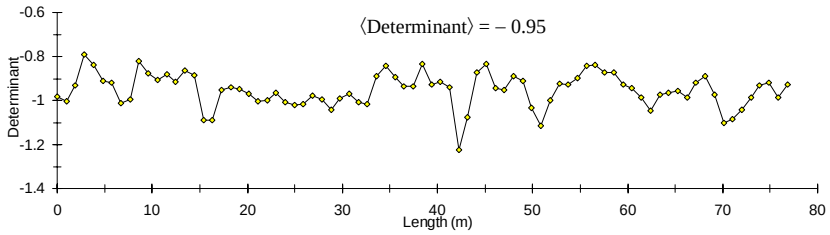

Figure 7.25 Calculated determinant of backscatter matrix from S-SMF 3 as a function of length.

7.5 Review on the POTDR measurement results

In this section, the DPD results calculated from POTDR will first be compared with the corresponding DGD values as measured in Chapter 6 (Table 6.1). This will help to understand the basic limitation in estimating the DGD in ordinary telecommunication fibres by using POTDR at a single frequency. Then the error in the measured SOP, using the single-channel POTDR and the four-channel POTDR, will be reconsidered, and lastly the depolarisation caused by the two-point resolution of the POTDR will be discussed.

In summary, we can say that, although the backscattered light is not fully polarised, the derived theory for twisted fibres describes the backscattered SOP evolution very well, as shown in the POTDR results in Sections 7.3 and 7.4.

7.5.1 Offset in DGD if estimated from the birefringence measured with POTDR

Table 7.1 lists the measured linear birefringence values using POTDR, measured for two S-SMFs and two DSFs at the centre wavelength $\lambda \approx 1.55$ μm. The DPD, as defined in Equation 3.19, has been calculated from these birefringence values. From the corresponding DGD values (Chapter 6, Table 6.1), the relative difference in the DGD to the DPD value (Equation 3.20) has been calculated. This difference in the DGD and DPD is in the range predicted from the calculation for S-SMFs with slight variations in their fibre parameters, but within the ITU-T recommendation. The offset Δ_τ predicted for S-SMF is between 40% and 60% at 1.55 μm as shown in Figure 3.15(b). For DSF, the prediction of the offset Δ_τ at 1.55 μm is ~ 45%, which agrees well with the offset measured, although the simulation assumes a step index profile and the measured fibre has a segmented profile.

It is interesting and promising that the prediction in the offset between the DGD and DPD values is quite close to that measured, which will help in the future to obtain an acceptable estimation of the expected DGD value from POTDR measurement results. However, we should also keep in mind that there is an error in both measurement methods, which makes it difficult to give an exact constant for the DPD to DGD conversion. The error in the birefringence estimated from the POTDR results can be said to increase with increasing linear birefringence, or twist for a fixed two-point resolution, whereas for the DGD results, using a polarimeter with tunable wavelength source, the relative error in the measured DGD decreases for increasing birefringence values (Chapter 6). The errors in Table 7.1 for the birefringence values, calculated from the POTDR data, have been taken as being due to the two-point resolution because the fibres have been measured close to zero twist.

Ideally, we would like to have a POTDR with tunable wavelength, which in order to see a change in the backscattered SOP on the Poincaré sphere, of say 10° at 10 metres distance for a fibre with $\delta\beta_L$ = 0.5 rad/m, would need a tuning range of about ±15 nm around λ = 1.55 μm, which is not practical by temperature tuning the laser.

Fibre Number	$\delta\beta_L$ (rad/m) from POTDR	DPD (ps/km) calculated from POTDR	DGD (ps/km) Table 6.1	$\Delta_\tau = 100\frac{DGD - DPD}{DGD}\%$
S-SMF 2	0.18 ± 0.01	0.15 ± 0.01	0.24 ± 0.1	38%
S-SMF 3	0.2 ± 0.04	0.16 ± 0.03	0.29 ± 0.1	50%
DSF 1	0.39 ± 0.15	0.32 ± 0.12	0.76 ± 0.1	58%
DSF 3	0.67 ± 0.15	0.55 ± 0.12	1.14 ± 0.1	52%

Table 7.1 Comparison of DPD and DGD values measured on the same fibres by using POTDR and Jones matrix eigenanalysis. The values are measured around the centre wavelength λ = 1.55 μm.

7.5.2 Measurement error with POTDR

Error analysis for polarimetry has been considered in detail in Section 4.4 and may be directly applied to POTDR, by considering the typical SNR error in the analysing optic and DOP as expected for POTDR. For a SNR of about 20 dB, as is about the case for the two polarimeters, the mean error in the SOP after Figure 4.9 is mainly due to the noise and has

been predicted from the numerical simulation to give an opening of the error angle $\langle\varepsilon\rangle$ of about 2° (for overall errors in the optics < 1° and fully polarised light).

Figure 7.26 shows the error angle ε calculated from two repeated POTDR measurement results on S-SMF 2 at about zero twist, which will give some indication of the repeatability of the measurement results. In Figure 7.26(a), the error angle for the single-channel POTDR is plotted versus length where it can be seen that the mean error value in the opening angle ε is about 3.8° with peak values up to 8°. The mean value is about twice that predicted above, but this is not only due to the lower DOP in the backscattered light, but also due to the relatively long measurement time needed for a single measurement (~ 30 minutes, Subsection 7.1.3) during which the measurement conditions of the launched SOP change slightly with time (see Subsection 7.1.4.5). The corresponding SOP measurements for S-SMF 2 are shown in Appendix B, Figure B.6(a). In Appendix B (Figure B.6(b)), the error angle ε of the single-channel POTDR is shown (measured on S-SMF 2) by using a fibre polariser at the output path in order to obtain a well polarised pulse. With this step, the error in the SOP could be reduced, below the predicted value, to about 2°. In Appendix B, there has also been an attempt to understand the error in the SOP due to the retardation error in the λ/4 plate which is less than ±1.5% at λ = 1.55 μm. Figure B.7 in Appendix B shows a plot of the error angle ε as a function of the SOP for an error in the retardation of ±1.5% but assuming zero noise, which showed that the average error over all the possible SOPs is $\langle\varepsilon\rangle$ = 0.44°.

Figure 7.26(b) shows the error angle ε measured for the four-channel POTDR with mean error of about 2.4° and peak values up to about 5°. The main error is now very close to the one predicted above for a SNR of 20 dB, and shows that, in order to further reduce the error in the SOP, the SNR of the POTDR has to be improved. The corresponding SOP measurement on S-SMF 2 is shown in Figure 7.23(a)

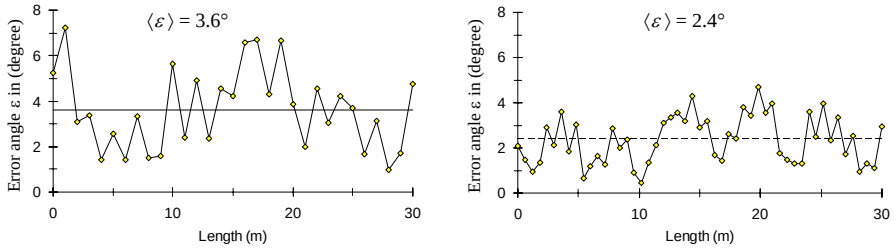

Figure 7.26 Error angle ε calculated from two repeated POTDR measurements on S-SMF 2. In (a) for the single-channel POTDR and in (b) for the four-channel POTDR.

In the presence of twist, the backscattered SOP evolution can be characterised by the periodicity of the SOP evolution, as defined in Equation (7.9), and by the shape of the SOP evolution, if plotted on the Poincaré sphere, as defined in Equation (7.10). For zero twist, the periodicity of the SOP evolution is determined by Equation (7.8) and the shape of the SOP evolution is a circle on the sphere. Assuming now that the measured backscattered SOP show one whole uniform evolution, the error in the linear and circular birefringence estimated from the POTDR data may be categorised in the following way:

(i) The error in the SOP periodicity may be taken as about $L \pm \Delta L \approx L \pm \Delta z$ with L given in Equation (7.9) for fibre with twist and in Equation (7.8) without, and Δz is given in Equation (7.4).

(ii) The error in the shape of the SOP evolution may be visualised as an error $\Delta\alpha$ in the angle α of the resultant rotation vector in forward or backward direction (Equation (7.10)) so that the average error in the measured SOP, away from the error free shape, is given by the opening angle $\langle\varepsilon\rangle$ as $\alpha \pm \Delta\alpha \approx \alpha \pm \langle\varepsilon\rangle/2$. The error angle $\langle\varepsilon\rangle$ is difficult to specify directly from the measurement conditions because it is an interplay of many errors, not only the noise (SNR) and linearity of the instrument (Subsection 7.1.4.3), but also the stability of the input SOP and the backscattered DOP. However, it may simply be determined as shown in Figure 7.26, from consecutive measurement results as carried out for the two POTDRs.

For the single-channel POTDR, the two-point resolution of about ±3 metres (Subsection 7.1.4.4) determines the error, at zero twist, for the estimated linear birefringence, which is the error given in Table 7.1 for S-SMF 3 and DSF 1 (±1 metre for S-SMF 2 and DSF 3). In the presence of twist, the error, as shown above, not only depends on the two-point resolution but also on the uncertainty in the measured SOP evolution, and the error in the estimated linear birefringence increases further with increasing twist.

7.5.3 Two-point resolution requirement as a function of the fibre birefringence

Figure 7.27(a) shows the DOP calculated using Equation 2.10 and Equation 2.11 by integrating the SOPs on the Poincaré sphere along arcs with different radii. For the arc with radius one, which is a great circle on the Poincaré sphere, the integrated DOP shows fully depolarised light for multiple rotations of 2π. For decreasing radius, the depolarisation as a

function of the integration angle gets smaller and for zero radius which represents just one point on the Poincaré sphere, the SOP stays fully polarised as expected for a fixed SOP. The last case is interesting because it would represent the case if light is launched into one of the PEMs of the fibre. Figure 7.27(b) shows the DOP for the measured backscattered SOP evolution integrated along S-SMF 2 as a function of length, at zero twist for two different input SOPs. For the first input SOP, which generated a circle in the backscattered SOP evolution of radius ~0.9 (see Figure 7.23(a)), the DOP of the integrated SOP evolves from about 0.85 to 0.2, with a minimum defined by the SOP periodicity at about L = 17 metre ($\delta\beta_L \approx 0.18 \approx \pi/L$ (rad/m)). For the other SOP, which generated a small circle with radius of about 0.46, the DOP of the integrated SOP is nearly fixed, as we would expect for such a small radius. The lower start DOP (at $l \approx 0$ m) in Figure 7.27(b) is due to the fact that the backscattered light is not fully polarised (~ 80%, see Figure 7.23(a)).

It is interesting to note that, although there were many trials, it was never possible to find an input SOP into the fibre under test perfectly aligned with the fibres PEMs. This may be due to the fact that for the fibre, for a combined forward-backward travel path, such PEMs do not exist due to the non-ideal scattering.

The inset in Figure 7.27(a) shows a magnified view of the DOP for the integrated SOP from just 20° of the arc. The two-point resolution for the POTDR should be such that the SOP in the fibre does not changes significantly within that range in order to obtain a DOP close to one. As a rule of the thumb, we may define the maximum two-point resolution, Δz, for POTDR assuming less than 20° angular movement on the Poincaré sphere as a function of the fibre birefringence $\delta\beta = \sqrt{\delta\beta_L^2 + (2\gamma - g\gamma)^2}$

$$\Delta z < \frac{20}{360}\frac{\pi}{\delta\beta} \tag{7.14}$$

From Equation (7.14), we may calculate the two-point resolution needed in order to measure an intrinsic linear birefringence of $\delta\beta_L$ = 3 rad/m, which is about the highest intrinsic linear birefringence we would expect in most S-SMFs and DSFs (Table 6.1). The spatial resolution needed would be about 0.06 metre. Further, as evident from Figure 4.9, for a POTDR we would like to have a DR of at least 20 dB in order to measure reasonably accurate backscattered SOPs along a fibre under test.

From Figure 7.27(a), it is now also possible to see that for the measured fibres (Section 7.4 and 7.5), the depolarisation in the backscattered SOP is not due to the two-point resolution of the used POTDRs. This we have experimentally confirmed by using shorter pulsewidths of 5 and 3 ns with the four-channel POTDR (longer averaging) again revealed about the same average DOP as measured using the 10 ns pulsewidth of about 70 to 80%. The reason as often mentioned throughout Section 7.4 and 7.5 may be found in the scattering effect of the fibre which seems to be non-ideal to a small degree. More investigation has to be carried out in clarifying this depolarisation effect due to scattering. If the exact scattering matrix is known, Equation (7.5) (which describes the backscattered SOP evolution) could be easily modified by using a more exact scatter matrix for $\mathbf{R}_M$. Ideally, we would like to have fully polarised light in the backscattered SOP evolution in order to minimise the error due to noise. However, the ideal scatter matrix as taken in analysing the measured backscattered SOPs seems to work well in revealing the linear and circular birefringence of the fibre.

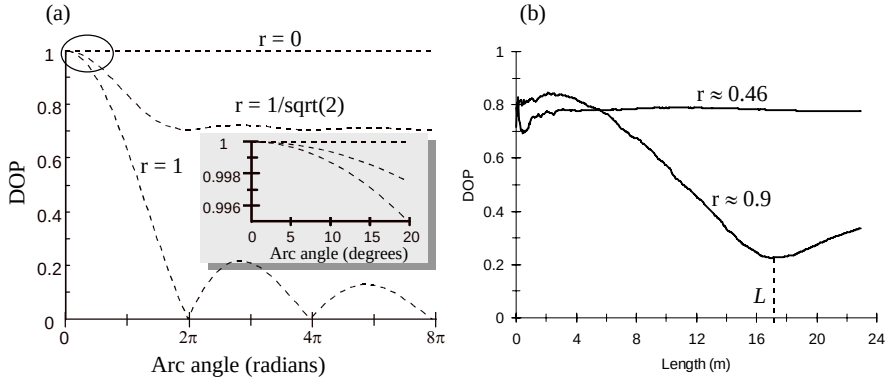

Figure 7.27 (a) Calculated DOP for integrated backscattered SOPs as a function of different arcs on the Poincaré sphere. (b) the DOP for the measured backscattered SOP evolution integrated along S-SMF 2 at zero twist for two different input SOPs, which showed a large (see Figure 7.23(a)) and a small circle on the Poincaré sphere.